

**BOLU ABANT IZZET BAYSAL UNIVERSITY
THE GRADUATE SCHOOL OF NATURAL AND APPLIED
SCIENCES**



**SYNTHESIS, STRUCTURAL CHARACTERIZATION AND
OPTICAL PROPERTIES OF MAGNESIUM PYROBORATE
NANOPARTICLES**

MASTER OF SCIENCE

LISKA FADLIYANI

BOLU, JUNE 2019

BOLU ABANT IZZET BAYSAL UNIVERSITY
THE GRADUATE SCHOOL OF NATURAL AND APPLIED
SCIENCES
DEPARTMENT OF CHEMISTRY



SYNTHESIS, STRUCTURAL CHARACTERIZATION AND
OPTICAL PROPERTIES OF MAGNESIUM PYROBORATE
NANOPARTICLES

MASTER OF SCIENCE

LISKA FADLIYANI

BOLU, JUNE 2019

APPROVAL OF THE THESIS

Synthesis, Structural Characterization and Optical Properties of Magnesium Pyroborate Nanoparticles submitted by **Liska FADLIYANI** and defended before the below named jury in partial fulfillment of the requirements for the degree of **Master of Science in Department of Chemistry, The Graduate School of Natural and Applied Sciences of Bolu Abant Izzet Baysal University** in **26.06.2019** by

Examining Committee Members

Signature

Supervisor
Prof. Dr. Ayşe Morkan
Bolu Abant Izzet Baysal University

Member
Assoc. Prof. Dr. Mecit Aksu
Düzce University

Member
Assoc. Prof. Dr. Bahadır Altıntaş
Bolu Abant Izzet Baysal University

Prof. Dr.Ömer ÖZYURT

Director of Graduate School of Natural and Applied Sciences

To my dearest family

DECLARATION

I hereby declare that all information in this document has been obtained and presented in accordance with academic rules and ethical conduct. I also declare that, as required by these rules and conduct, I have fully cited and referenced all material and results that are not original to this work.



Liska FADLIYANI

ABSTRACT

SYNTHESIS, STRUCTURAL CHARACTERIZATION AND OPTICAL PROPERTIES OF MAGNESIUM PYROBORATE NANOPARTICLES

MSC THESIS

LISKA FADLIYANI

**BOLU ABANT IZZET BAYSAL UNIVERSITY GRADUATE SCHOOL OF
NATURAL AND APPLIED SCIENCES**

DEPARTMENT OF CHEMISTRY

(SUPERVISOR: PROF. DR. AYŞE MORKAN)

BOLU, JUNE 2019

In this study, Pure $Mg_2B_2O_5$ were successfully synthesized using different kinds of organic fuels (carbohydrazide, citric acid, glycine, HMDA, HMTA, tartaric acid and urea) via Solution Combustion Synthesis (SCS) method. The structural and optical properties of as-prepared products were comparatively characterized by Infrared spectroscopy (FTIR), X-Ray Powder Diffraction (XRD) and Ultra Violet- Visible spectroscopy (UV-VIS) techniques.

During the process of preparation, $Mg(NO_3)_2 \cdot 6H_2O$, 5wt% excess H_3BO_3 , and fuel were used as the starting materials. The effects of fuels and temperature on the structural properties of the products were examined by XRD studies. It is shown that at low temperatures between 400 and 800°C, $Mg_2B_2O_5$ was resulted in monoclinic phase except for carbohydrazide fuel. At 900°C, the transformation of monoclinic phase of $Mg_2B_2O_5$ into triclinic phase was obtained. Most accurately, the single phase triclinic was acquired for all fuels at 1000°C. In the analysis of infrared spectra, the bands around 680 cm^{-1} and 720 cm^{-1} represent to the B-O-B bending and the bands assigned at 1175 cm^{-1} , 1290 cm^{-1} and 1490 cm^{-1} belong to stretching vibrations of trigonal BO_3 confirmed the formation of magnesium pyroborate.

The effects of fuels and heating temperatures on optical properties of $Mg_2B_2O_5$ were further examined using Ultra Violet- Visible spectroscopy (UV-VIS). It was found that the optical band gap energy of the products decreases as the temperature increases. The calculated optical band gap energy was attained at range of 4.66-4.91 eV for different fuels. The lowest band gap of $Mg_2B_2O_5$ was detected for citric acid fuel whereas highest value was found for urea fuel.

KEYWORDS: Solution Combustion Synthesis, Magnesium Pyroborate, Suanite, organic fuel

ÖZET

MAGNESYUM PİROBORAT NANOPARÇACIKLARIN SENTEZİ, YAPISAL KARAKTERİZASYONU VE OPTİK ÖZELLİKLERİ

YÜKSEK LİSANS TEZİ

LİSKA FADLIYANI

BOLU ABANT İZZET BAYSAL ÜNİVERSİTESİ

FEN BİLİMLERİ ENSTİTÜSÜ

KİMYA ANABİLİM DALI

(TEZ DANIŞMANI: PROF. DR. AYŞE MORKAN)

BOLU, HAZİRAN - 2019

Bu çalışmada, saf $Mg_2B_2O_5$, farklı türdeki organik yakıtlar (karbohidrazid, sitrik asit, glisin, HMDA, HMTA, tartarik asit ve üre) kullanılarak Çözeltide Yanma Sentez (SCS) yöntemi kullanılarak başarılı bir şekilde sentezlendi. Hazırlanan ürünlerin yapısal ve optik özellikleri karşılaştırmalı olarak, Kızılötesi spektroskopisi (FTIR), X-Işını Tozu Kırınımı (PXRD), ve Ultra Violet-Görünür spektroskopisi (UV-VIS) teknikleri ile karakterize edildi.

Hazırlık sürecinde, başlangıç materyali olarak $Mg(NO_3)_2 \cdot 6H_2O$, %5 fazla H_3BO_3 ve organik yakıt kullanılmıştır. Yakıtların ve sıcaklığın ürünler üzerindeki etkileri XRD ile incelenmiştir. Düşük sıcaklıklarda (400-800°C arası), karbohidrazid yakıtı ile elde edilen ürün hariç, $Mg_2B_2O_5$ 'in monoklinik faz ile sonuçlandığı görülmüştür. 900°C'de ise $Mg_2B_2O_5$ 'in monoklinik fazdan triklinik faza dönüşümü elde edilmiştir. Kesin bir şekilde tüm yakıtlarda, tek fazlı triklinik $Mg_2B_2O_5$ 1000°C'de elde edilmiştir. Infrared spektrumlarının analizinde, trigonal BO_3 e ait, 680 cm^{-1} ve 720 cm^{-1} de B-O-B eğilme ve 1175 cm^{-1} , 1290 cm^{-1} , 1490 cm^{-1} de gerilme titreşimlerinin gözlenmesi ile magnezyum piroborat oluşumu desteklenmektedir.

Yakıtların ve ısıtma sıcaklıklarının $Mg_2B_2O_5$ 'in optik özellikleri üzerindeki etkileri Ultra Violet-Görünür spektroskopisi (UV-VIS) kullanılarak incelenmiştir. Ürünlerin optik bant aralığı enerjisinin sıcaklık arttıkça düştüğü gözlenmiştir. Hesaplanan optik bant aralık enerjisi 4.66-4.91 eV aralığında bulunmuştur. $Mg_2B_2O_5$ için, en düşük bant aralığı sitrik asit, en yüksek bant aralığı üre yakıtı ile elde edilmiştir.

ANAHTAR KELİMELELER: Çözeltide Yanma Sentez Yöntemi, Magnezyum piroborat, suanite, organik yakıt

TABLE OF CONTENTS

	<u>Page</u>
ABSTRACT	v
ÖZET	vi
TABLE OF CONTENTS	vii
LIST OF FIGURES	viii
LIST OF TABLES	ix
LIST OF ABBREVIATIONS ANDSYMBOLS	x
1. INTRODUCTION	1
1.1 NANOPARTICLES	1
1.2 BORATES	2
1.2.1 History and Uses of Borates	2
1.2.2 Classification and Structure of Borates	4
1.2.3 Pyroborates	6
1.2.3.1 Metal Pyroborates	7
1.3 SYNTHESIS METHOD OF BORATES	17
1.3.1 Solid State Method.....	17
1.3.2 Solid Gas Method	17
1.3.3 Solution Method	18
1.3.3.1 Solution Combustion Synthesis (SCS)	18
2. AIM AND SCOPE OF THE STUDY	22
3. MATERIALS AND METHODS	23
3.1 CHEMICALS	23
3.2 INSTRUMENTS	24
3.2.1 Fourier Transform Infrared Spectrophotometer	24
3.2.2 X-ray Powder Diffractometer	24
3.2.3 UV- VIS Spectrometer.....	24
3.2.4 Furnace.....	24
3.3 METHODS	25
3.3.1 Synthesis of Magnesium Pyroborates.....	25
4. RESULTS AND DISCUSSION	27
4.1 Synthesis of Pure Magnesium Pyroborates	27
4.1.1 Structural Characterization Studies of Pure Mg ₂ B ₂ O ₅	32
4.1.1.1 FT-IR Spectroscopy Studies	32
4.1.1.2 Powder X-Ray Diffraction (PXRD) Studies	42
4.1.1.3 UV-VIS Spectroscopy Studies.....	55
5. CONCLUSIONS	63
6. REFERENCES	64
7. CURRICULUM VITAE	69

LIST OF FIGURES

	<u>Page</u>
Figure 1.1. Source of Borate Minerals	3
Figure 1.2. Structures of Boron-Oxygen Arrangements	5
Figure 1.3. Structures of Borates.....	6
Figure 1.4. Suanite Mineral.....	8
Figure 1.5. Crystal Structure of Magnesium Pyroborate	8
Figure 1.6. Structure of Monoclinic and Triclinic Phase of $Mg_2B_2O_5$	10
Figure 3.1. Schematic Diagram of $Mg_2B_2O_5$ Synthesis	25
Figure 4.1. Digital Photos of $Mg_2B_2O_5$ with Citric Acid as Fuel	30
Figure 4.2. Digital Photos of $Mg_2B_2O_5$ with Citric Acid as Fuel	30
Figure 4.3. Digital Photos of $Mg_2B_2O_5$ with Glycine as Fuel.....	30
Figure 4.4. Digital Photos of $Mg_2B_2O_5$ with HMDA as Fuel	30
Figure 4.5. Digital Photos of $Mg_2B_2O_5$ with HMTA as Fuel.....	31
Figure 4.6. Digital Photos of $Mg_2B_2O_5$ with Urea as Fuel.....	31
Figure 4.7. Digital Photos of $Mg_2B_2O_5$ with Tartaric Acid as Fuel.....	31
Figure 4.8. FT-IR Spectra of Synthesis $Mg_2B_2O_5$ Using All Fuels	33
Figure 4.9. FT-IR Spectra of $Mg_2B_2O_5$ at 400°C Using All Fuels.....	34
Figure 4.10. FT-IR Spectra of $Mg_2B_2O_5$ at 500°C Using All Fuels.....	35
Figure 4.11. FT-IR Spectra of $Mg_2B_2O_5$ at 600°C Using All Fuels.....	36
Figure 4.12. FT-IR Spectra of $Mg_2B_2O_5$ at 700°C Using All Fuels.....	37
Figure 4.13. FT-IR Spectra of $Mg_2B_2O_5$ at 800°C Using All Fuels	38
Figure 4.14. FT-IR Spectra of $Mg_2B_2O_5$ at 900°C Using All Fuels.....	39
Figure 4.15. FT-IR Spectra of $Mg_2B_2O_5$ at 1000°C Using All Fuels.....	41
Figure 4.16. PXRD Patterns of Synthesis $Mg_2B_2O_5$ Using All Fuels.....	43
Figure 4.17. PXRD Patterns of $Mg_2B_2O_5$ Heated at 400°C Using All Fuels... 44	44
Figure 4.18. PXRD Patterns of $Mg_2B_2O_5$ Heated at 500°C Using All Fuels... 45	45
Figure 4.19. PXRD Patterns of $Mg_2B_2O_5$ Heated at 600°C Using All Fuels... 46	46
Figure 4.20. PXRD Patterns of $Mg_2B_2O_5$ Heated at 700°C Using All Fuels... 49	49
Figure 4.21. PXRD Patterns of $Mg_2B_2O_5$ Heated at 800°C Using All Fuels... 50	50
Figure 4.22. PXRD Patterns of $Mg_2B_2O_5$ Heated at 900°C Using All Fuels... 51	51
Figure 4.23. PXRD Patterns of $Mg_2B_2O_5$ Heated at 1000°C Using All Fuels. 52	52
Figure 4.24. Crystallite Size of $Mg_2B_2O_5$ Obtained at 700°C-1000°C	54
Figure 4.25. UV-VIS Absorbance Spectra of $Mg_2B_2O_5$ at 800°C	57
Figure 4.26. UV-VIS Reflectance Spectra of $Mg_2B_2O_5$ at 800°C	57
Figure 4.27. UV-VIS Absorbance Spectra of $Mg_2B_2O_5$ at 900°C	58
Figure 4.28. UV-VIS Reflectance Spectra of $Mg_2B_2O_5$ at 900°C	58
Figure 4.29. UV-VIS Absorbance Spectra of $Mg_2B_2O_5$ at 1000°C	59
Figure 4.30. UV-VIS Reflectance Spectra of $Mg_2B_2O_5$ at 1000°C	59
Figure 4.31. Optical Band Gap Energy of $Mg_2B_2O_5$ obtained at 800°C-1000°C 60	60
Figure 4.32. Optical Band Gap Energy of $Mg_2B_2O_5$ at 800°C	61
Figure 4.33. Optical Band Gap Energy of $Mg_2B_2O_5$ at 900°C	62
Figure 4.34. Optical Band Gap Energy of $Mg_2B_2O_5$ at 1000°C	62

LIST OF TABLES

	<u>Page</u>
Table 1.1. Common Borate Minerals	4
Table 1.2. The Properties of Monoclinic and Triclinic $Mg_2B_2O_5$	10
Table 1.3. The Most Common Used Starting Materials in SCS	20
Table 4.1. Observation during the Preparation of Pure $Mg_2B_2O_5$	27
Table 4.2. FTIR Assignment of $Mg_2B_2O_5$ with all fuels and wavenumbers(cm^{-1}) at $1000^\circ C$	40
Table 4.3. Crystallite Size of $Mg_2B_2O_5$	53
Table 4.4. UV-VIS Absorbance Spectra Wavelength of $Mg_2B_2O_5$	55
Table 4.5. UV-VIS Reflectance Spectra Wavelength of $Mg_2B_2O_5$	56
Table 4.6. Optical Band Gap Energy of Pure $Mg_2B_2O_5$	61

LIST OF ABBREVIATIONS ANDSYMBOLS

CA	: Citric Acid
CH	: Carbohydrazide
EDS	: Energy Dispersive X-Ray Spectroscopy
FTIR	: Fourier Transform Infrared Spectrometer
HMDA	: Hexamethylenediamine
HMTA	: Hexamethylenetetramine
ICDD	: International Centre for Diffraction Data
PXRD	: Powder X-Ray Diffractometer
RE	: Rare Earth
SAED	: Selected Area Diffraction
SCS	: Solution Combustion Synthesis
TA	: Tartaric Acid
TEM	: Transmission Electron Microscopy
UV-VIS	: Ultraviolet- Visible

ACKNOWLEDGEMENTS

I would like to express my sincere gratitude to my supervisor Prof. Dr. Ayşe MORKAN for the continuous support and encourage me during my M.Sc study, for her insightful comments, which incented me to widen my research, for her patience, motivation and immense knowledge. Without her professional guidance, it would not be possible for me to finalize this thesis.

I would also like to thanks Prof. Dr. İzzet MORKAN for always encourage and motivate me during this study.

I would also like to thanks Arş. Gör. Dr. Seda KARABOĞA and Öğr. Gör. Nevin SOYLU KOÇ, for their help and time providing the instruments for the analysis. Especially, I would like thank to Gülden ÖZEN KAHVECİ and Umut KESKİN for their helps.

I would like thank my labmate, Fatma YALÇIN for the stimulating discussions and feedbacks, for spending days and nights working together before deadlines, and for all the fun we have had in the last two years during this study.

I would also like to acknowledge Rizky Amallia as the second reader of this thesis and I am gratefully indebted toher for her valuable comments on this thesis.

Heartfelt thanks goes to my best friends, Mangga's members; Puji Esa Suci and Rizka Nurdhillah for listening, entertained and give me strengths despite the long distance between us. Special thanks to Sufia Umami Fadhal for the encouragement, friendship and for always be there for me. Special shout out goes to EXO's members who always entertain me, spread the positive energy and cheer me up with their music during this entire process.

Last but not least, I want to express my very profound gratitude to my family: my parents, Bukhari USMAN and Lismawati, my brothers and sister; Qishan FADHILLAH, Raffi FACHREZI and Aqila FANCILIYA for providing me with unstoppable encouragement and unflinching supports during my years of study and throughout research and writing processes of this thesis. This accomplishment would not have been possible without them.

1. INTRODUCTION

1.1 NANOPARTICLES

Nanotechnology is the study that employs the molecular and atomic scale of matter in $1/10^{-9}$ meter or generally express in term of nanometer (nm). Nanoparticle covers in the range of 1 to 100nm and is the most essential element in the formation of nanostructure. It consists of an atom or more that can advertise the properties of size-dependent to be differentiated from bulk materials. According to their morphology, nanoparticle are known for its sphericity, flatness and its large aspect ratio particle; nanotubes and nanowires, and low aspect ratio particle; oval, prism, cubic, pillar, spherical and helical. Nanoparticles can be classified according to their morphology, chemical properties and size. There are some types of nanoparticles that can be differed on the basis of their physical and chemical characteristic namely, semiconductor nanoparticles, lipid and carbon based nanoparticles, metal nanoparticles, ceramic nanoparticles, polymeric nanoparticles and etc. Chiefly, they are classified into two types which are inorganic and organic nanoparticles that included semiconductor and carbon nanoparticles, respectively (Buzea et al., 2007; Horikoshi and Serpone, 2013; Khan et al., 2017)

Recent years, inorganic nanoparticles have been expanded and synthesized in many research due to their interesting physical properties that include magnetic properties, electronic properties, size- dependent properties and catalytic properties. Although it consider as simple molecule that small in size, actually the structure of nanoparticles are quite complex. The behaviors of nanoparticles depend on the component of the molecules or materials which resulted in the high volume ratio and high surface area. Many different methods have been applied in the preparation of nanoparticles. These methods are widely classified into two methods which are top down method; synthesized the nanoparticles started from large substance and bottom up method; synthesized the nanoparticles by using simpler molecule as starting materials (Cristian et al., 2008; Benelmekki, 2015; Heera and Shanmugam, 2015).

Nanoparticles have been utilized in many area such as in communication and information technologies, water decontamination, power engineering, environmental engineering, chemical industry, industrial engineering, cosmetics and pharmaceuticals, especially nanoparticles are used in the medical application; diagnostic tools for cancer treatment, gene delivery and drugs delivery. In more additions, nanoparticles have also shown their potential uses as sports good, textile, cosmetics, coatings, bioanalysis and detectors, light sources and many of their uses have been increase and studied continually (Buzea et al., 2007; Cristian et al., 2008; Jeevanandam et al., 2018)

1.2 BORATES

Borates are defined as the compound consisting of boron and oxygen or also known as boric oxide. Boron which is the fifth element of periodic table is an element that does not form in its elemental form naturally and is the only non-metallic element that has electron-deficiency characteristic. Boron also has a high affinity for oxygen; boron atoms in borates combine with oxygen and form a strong covalent bond with oxygen. Hence, borates are generally expressed in B_2O_3 and also defined as the salt of boric acid (Kistler and Helvaci, 1994).

1.2.1 History and Uses of Borates

Borates have been discovered in many countries such as Egypt, China, Tibet, Venice, United State and Turkey since thousands years ago as shown in Figure 1.1. Borates minerals were firstly used during the ancient time from at least 8th century as a flux for refining gold and silver. Occasionally, borates were utilized in wide range of used such as medicines, wood preservatives, ceramic glaze and metal fluxes (Kistler and Helvaci, 1994).

Despite the fact that there are more than 200 minerals that contain boric oxide, borates are used widely in industrial and domestic application as mineral. The borates minerals that mostly used in industry are borax, ulexite and celemanite. These mineral was dominated in United State, South America and Turkey. The list of

the most important and common minerals commercially are reported (Briggs, 2001) (Table 1.1).

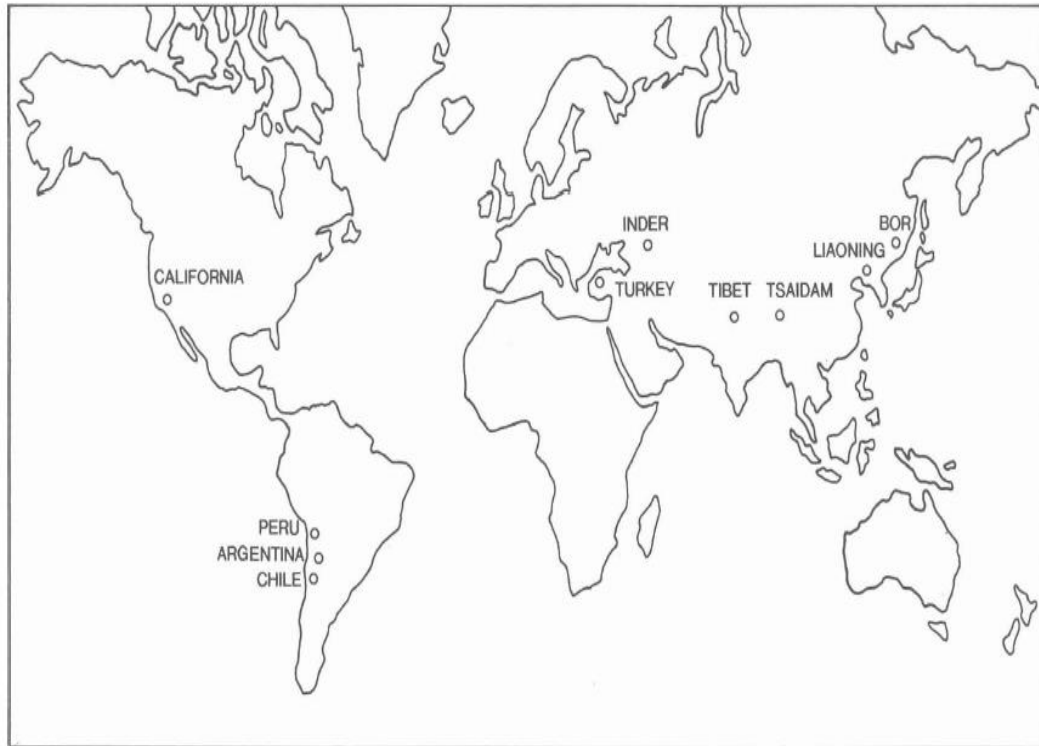


Figure 1.1. Source of Borate Minerals

Although borates have low concentrations in nature, the boron-containing borates are generally found in soil, rocks and water. Most borates are discovered in the mixture of clays, mudstones, tuffs, and limestone from the minerals springs and hydrothermal activity alongside the volcanic activity. Nowadays, Borates are applied in large scale of area due to their unique characteristics namely, light weight, heat and impact resistance, chemical durability and great mechanical strength. Borates are used mostly as fiberglass insulation, textile fiberglass, enamels and frits and ceramic glaze (Woods, 1994). Borates are also applied and used in daily and environmental usage; detergent and bleach, flame retardants, fertilizer and many agricultural products. Furthermore, borates are also utilized in aerospace, various household appliance, medical application and metallurgy (Briggs, 2001).

Table 1.1. Common Borate Minerals

Mineral	Empirical Formula	B₂O₃ content, wt%	Location of minerals
Borax	Na ₂ B ₄ O ₇ ·10H ₂ O	36.5	United state, Turkey, Argentina
Kernite	Na ₂ B ₄ O ₇ ·4H ₂ O	51.0	United-State
Ulexite	NaCaB ₅ O ₉ ·8H ₂ O	43.0	Turkey, South America
Colemanite	Ca ₂ B ₆ O ₁₁ ·5H ₂ O	50.8	Turkey
Inderite	Mg ₂ B ₆ O ₁₁ ·15H ₂ O	37.3	Kazakhstan
Szaibelyite (ascharite)	Mg ₂ B ₂ O ₅ ·H ₂ O	41.4	China
Suanite	Mg ₂ B ₂ O ₅	46.3	China
Datolite	Ca ₂ B ₂ Si ₂ O ₉ ·H ₂ O	21.8	Russia

1.2.2 Classification and Structure of Borates

The first chemical classification of borates was projected by Herman and revised by Menzel. According to Herman and Menzel, Borates are assigned into three types named as metaborates, diborates and pentaborates as the boron atom is a tetra coordinated atom. Furthermore, classification of borates was also proposed by Carpeni who differentiate borates according to the boron atoms' in anion and according to the basicity of their anion. According to Carpeni, the structural formula

of boron atoms in borates are in triangular coordination and are divided into three groups namely; orthoborates or metaborates, tetraborates, and pentaborates (Bokii and Kravchenko, 1967)

The best clarified borate structure is defined to be orthoboric acid which is consisted of triangular BO_3 and has 1.361\AA bond distance of B-O (Block et al., 1959). Moreover, the crystal structure of borates also can be distinguished by the following characteristics:

- i. In borate crystal structure, Boron atoms can have trigonal coordination and tetrahedral coordination to oxygen (O^{2-}) or hydroxyl group (OH^-)
- ii. Both triangle (BO_3) and tetrahedra (BO_4) can be combined to each other by oxygen to form a rigid boron-oxygen bond.
- iii. The fundamental building blocks of borates can be polymerized into complex polyanions such as chain, layers, and networks (Yuan and Xue, 2007)

The Boron-oxygen bond arrangements in borates are varies according to its triangular BO_3 and tetrahedral BO_4 coordination, shown in Figure 1.2. The Boron-Oxygen bond lengths of both coordinates are different as the boron atom combined in different manner with oxygen. The B-O bond length of triangular BO_3 varies in the range of 1.28\AA to 1.43\AA . In addition, triangular BO_3 has shorter B-O bond length than tetrahedral BO_4 . Average bond lengths of triangular and tetrahedral are 1.37\AA and 1.48\AA , respectively. The change of the bond distance is due to the change in the bond order in coordinate structure (Coulson and Dingle, 1968).

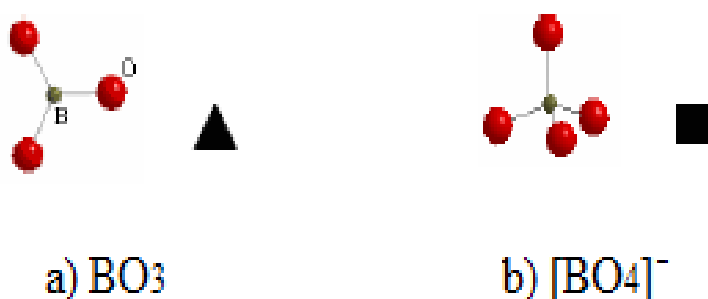


Figure 1.2. Structures of Boron-Oxygen Arrangements

Triangular planar BO_3 coordination can be arranged in different way to form oxyanions containing boron, such as monomeric triangular $[\text{BO}_3]^{3-}$, binuclear triangular planar $[\text{B}_2\text{O}_5]^{4-}$, Triangular cyclic $[\text{B}_3\text{O}_6]^{3-}$ and polynuclear infinite chain $[(\text{BO}_2)]_n$, (Figure 1.3). These arrangements are also known as orthoborate, pyroborate and metaborate, respectively.

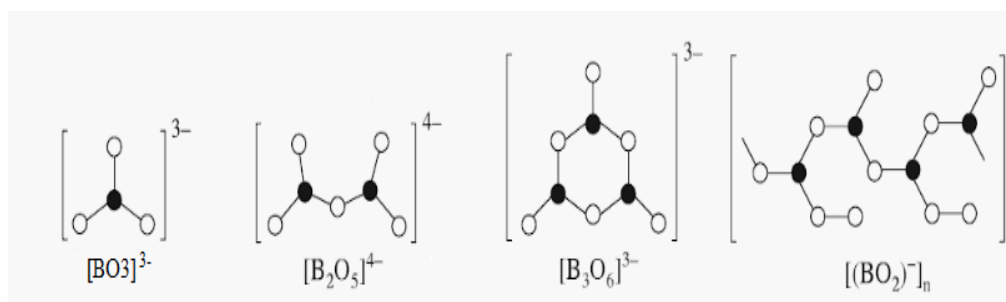


Figure 1.3. Structures of Borates

The examples of mineral or compound of monomeric triangular BO_3 coordination are Ketoite $\text{Mg}_3(\text{BO}_3)_2$ and $\text{CaSn}^{\text{IV}}(\text{BO}_3)_2$. Pyroborates $\text{Mg}_2(\text{B}_2\text{O}_5)$, $\text{Co}_2^{\text{II}}(\text{B}_2\text{O}_5)$ and $\text{Fe}_2^{\text{II}}(\text{B}_2\text{O}_5)$ are the examples of minerals with binuclear triangular BO_3 coordination. Triangular Cyclic found in NaBO_2 and KBO_3 minerals (Sahoo et al., 2012).

1.2.3 Pyroborates

In Crystal structure of crystalline borates, triangular planar BO_3 and tetrahedral BO_4 can be combined to each other to form boric oxide group. Pyroborates is one of the complex borates alongside orthoborate and metaborate. It is formed when two triangular BO_3 link to each other by sharing an oxygen atom. It generally expressed in the basis of $[\text{B}_2\text{O}_5]^{4-}$ as shown in Figure 1.4. Unlike orthoborates, the structure of BO_3 in pyroborates is not perfectly planar (Arora, 2005; Madan and Tuli, 2007).

1.2.3.1 Metal Pyroborates

Metal borates have drawn great attentions due to its fascinating properties, such as corrosion-resisting, thermal-resisting, high mechanical strength and high efficient of elasticity (Elssfah et al., 2007). These properties allow metal borate to utilize in many areas as in reinforcement in the electronic, ceramic, wide band gap semiconductor, anti-wear additive and plastics or the matrix alloy of aluminum/magnesium (Zhu et al., 2014). For these reasons, many metal borates have been synthesized and studied in the past decades, namely lithium borates, potassium borates, rubidium borates, cesium borates, beryllium borates, magnesium borates, strontium borates, iron borates, copper borates, zinc borates, cadmium borates, mercury borates, aluminum borates, thallium borates, etc (Emeléus, 1982).

Among those metal borates, this study is focused on magnesium borates especially magnesium pyroborate, $Mg_2B_2O_5$. Different types of magnesium borates; $Mg_3B_2O_6$, MgB_4O_7 and $Mg_2B_2O_5$ have been synthesized successfully by many researchers. Magnesium borates have attracted a great amount of attention due to their potential application such as thermo-luminescence phosphors, cathode ray tube screens, X-ray screens, catalyst for hydrocarbon conversion, good anti-wear and anti-corrosion material, anti-thermal shock agent. It may be used as electroconductive treating agent and reinforcing materials for plastics (Došler et al., 2010; Elssfah et al., 2007; Qasrawi et al., 2005).

Magnesium pyroborates are firstly discovered in 1939 by Watanabe in Holkol mine of Suan districts, North Korea alongside with ketoite and other borates minerals. Magnesium pyroborate contain 53.66% MgO and 46.34% B_2O_3 . Magnesium pyroborate is white in color, has a silky luster, difficult to fuse and perfectly colorless in fine piece, shown in Figure 1.4.



Figure 1.4. Suanite Mineral

The structure of magnesium pyroborates consist of Mg^{2+} ion and pyroborates group $[B_2O_5]^{4-}$. The magnesium ion in $Mg_2B_2O_5$ was surrounded octahedrally by oxygen atoms (Figure 1.5). $Mg_2B_2O_5$ is a dimorphous. It has two different crystallography forms as monoclinic phase and triclinic phase (Watanabe, 1953).

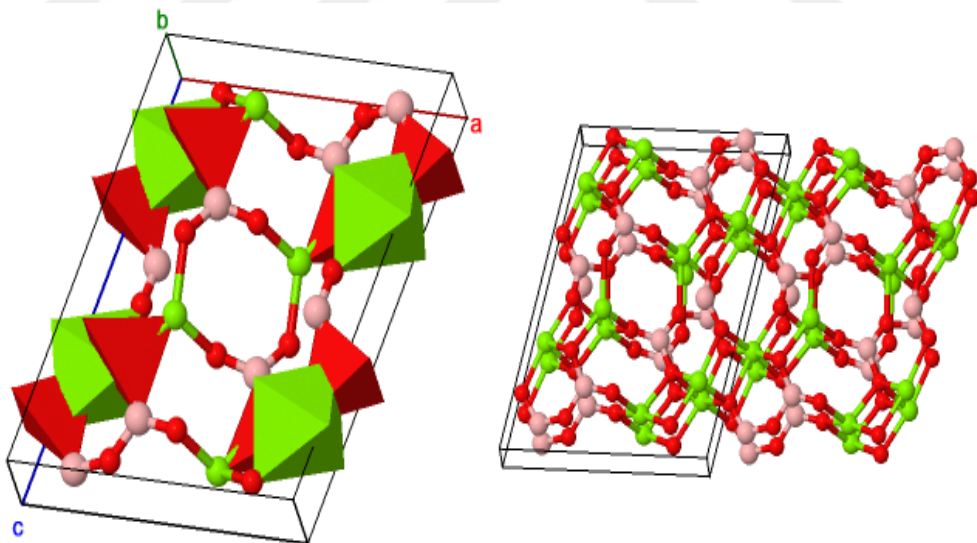


Figure 1.5. Crystal Structure of Magnesium Pyroborate

The crystal structure of $Mg_2B_2O_5$ was firstly described by Takeuchi (1952) with rotation and Wiesenberger photographs Mo $K\alpha$ ($\lambda=0.710$). According to Takeuchi's studies, the crystal structure of $Mg_2B_2O_5$ is monoclinic phase. Suanite, which is the monoclinic form of $Mg_2B_2O_5$ has the cell parameter dimension as $a=12.10\pm 0.05\text{\AA}$, $b=3.12\pm 0.02\text{\AA}$, $c=9.36\pm 0.05\text{\AA}$, $\beta= 104^\circ 21'$, $Z=4$ and P21/c space group. It crystal is parallel to [010] and has axial ratio $a:b:c = 3.880:1:3.000$. Its hardness and specific gravity is 5.5 and 2.19, respectively (Takeuchi, 1952).

The triclinic form of $Mg_2B_2O_5$ was firstly observed when the nature mineral of $Mg_2B_2O_5$ was heated at 630°C . Although, the synthesis of $Mg_2B_2O_5$ was firstly reported by W. Gutler, the synthesized crystal structure was studied by Davis and Knight. Based on Wanatabe's synthesis by cooling the fused mass of MgO and B_2O_3 slowly, the unit cell of triclinic phase has dimension $a=3.12\text{\AA}$, $b=5.93\text{\AA}$, $c=9.03\text{\AA}$ with axial angles $\alpha=103.9^\circ$, $\beta=90.9^\circ$, $\gamma=92.0^\circ$ (Watanabe, 1953). As pyroborates group are formed by triangular coordination of boron atom with oxygen atoms that consisted of three coplanar bonds applying Sp^2 hybridization, in $Mg_2B_2O_5$ the B-O-B angle appears to be 134.5° . Also, the two triangular BO_3 are non-identical to each other, has unsymmetrical bond length (Block et al., 1959).

Guo et al has also studied and synthesized the monoclinic forms and triclinic forms of $Mg_2B_2O_5$ based on Mg_4O_{18} tetramers obtained from the mixture of boric acid (H_3BO_3) and $Mg_2(OH)_2CO_3$. Boron atoms held the tetrameric chains of Mg to form B_2O_5 groups and these tetramers are composed of four octahedral of Mg linked by three shared edges and connected by sharing O-O edge forming chains that projected in different views and extending along [010] plane and [001] plane for monoclinic form and triclinic form, respectively as shown in Figure 1.6. Properties of both forms of $Mg_2B_2O_5$ are described in Table 1.2 (Guo et al., 1995a, 1995b).

Table 1.2. The Properties of Monoclinic and Triclinic $\text{Mg}_2\text{B}_2\text{O}_5$

	Monoclinic $\text{Mg}_2\text{B}_2\text{O}_5$	Triclinic $\text{Mg}_2\text{B}_2\text{O}_5$
Space group	$P2_1/c$	$\bar{P}1$
Z	4	2
Unit cell:		
a	9.197 Å	6.149 Å
b	3.1228 Å	9.221 Å
c	12.303 Å	3.121 Å
Axial angle		
α	-	90.29°
β	104.26°	92.23°
γ	-	104.30°
Volume	342.5 Å ³	171.4 Å ³

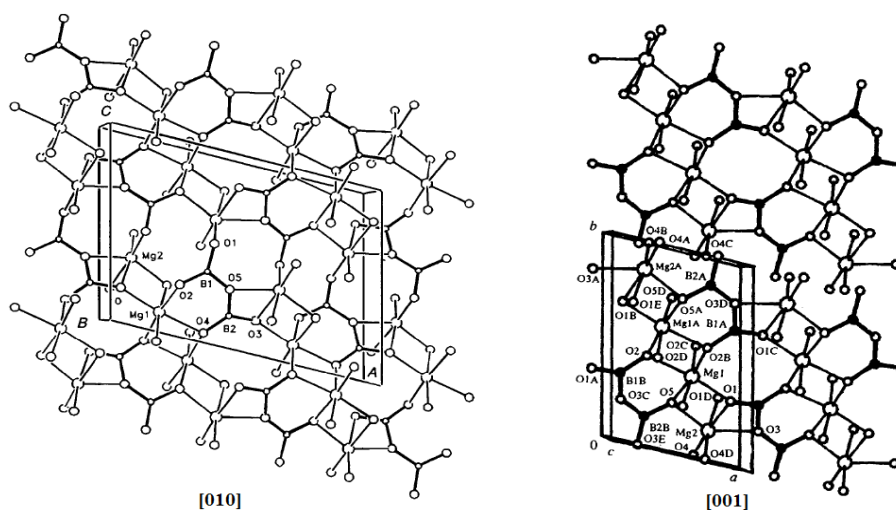


Figure 1.6. Structure of Monoclinic and Triclinic Phase of $\text{Mg}_2\text{B}_2\text{O}_5$

Recent years, the synthesis of Magnesium Pyroborates has been carried out in many different methods as magnesium pyroborates are well known for their fascinating properties. Various methods have been studied extensively by many scientists and were mostly focused on its nanomaterial structures such as nanowires, nanotubes, and nanorods. In 1988, Kitamura et al have synthesized the $Mg_2B_2O_5$ via Flux method where NaCl was used as a flux. The effects of the NaCl on the crystal formation of $Mg_2B_2O_5$ were determined. MgO, B_2O_3 and NaCl were used as the reactants and various molar ratio of Mg/B were applied. The mixed materials were heated at $850^\circ C$ for 5hours. The crystal structure of $Mg_2B_2O_5$ was characterized and found to be monoclinic phase in fibrous form (Kitamura et al., 1988).

Using BI_3 and H_3BO_3 vapor mixture as precursors, single crystal $Mg_2B_2O_5$ nanowires have been synthesized using chemical vapor deposition by heating MgO (1 0 0) substrates coated with Pt/Pd nanofilms as catalyst. The resulted that the nanowires growth mechanism is in VLS-type process and are wide gap semiconductor (Li et al., 2004).

Qasrawi et al. (2005) has reported the preparation of Magnesium Pyroborates which lead to highly pure triclinic $Mg_2B_2O_5$ after annealing at $1250^\circ C$ for 3 hours by using partial precipitation technique with $Mg(OH)_2$ and H_3BO_3 as starting materials. The single phase $Mg_2B_2O_5$ reportedly has band gap width 4.72eV and resistivity activation energy of 0.71eV (high temperature) and 0.13 (low temperature). Furthermore, it is also shows a p-type conductivity.

Using $Mg_2(NO_3)_2 \cdot 6H_2O$, H_3BO_3 and citric acid as initial materials, $Mg_2B_2O_5$ has been synthesized by applying sol-gel method. The homogenous mixtures were heated at $950^\circ C$. The morphology and structures of products were investigated by XRD, SEM, and TEM (Jiang et al., 2006).

Single-phase $Mg_2B_2O_5$ nanorods have also been synthesized by directly calcining the starting materials which are $Mg(OH)_2$ and H_3BO_3 . The reaction were run without further purification and were mixed together to form homogenized mixture which then heated at $900^\circ C$ for 3hours in a resistance-heating furnace. The characterization and the growth mechanism of $Mg_2B_2O_5$ were also presented (Elssfah et al., 2007).

Mg₂B₂O₅ nanowires have been also synthesized by Zeng et al. (2008). Single crystalline Mg₂B₂O₅ was successfully prepared by heating the mixture of tablet of Mg(BO₂)₂ and graphite directly in the vacuum furnace for 1 hour at higher temperature between 1150-1250°C. The growth of Mg₂B₂O₅ nanowires at different heating temperatures, thermal treatment times and the effects of the existence of graphite on its preparation were investigated. It reported that only Mg(BO₂)₂:graphite can formed the Mg₂B₂O₅ and the best outcome were observed at 1:2 molar ratio. Also, the best results were achieved when the materials heated at 1200°C for an hour. The nanowires of 120-180 nm and length ~0.2 mm were attained.

In 2008 Mg₂B₂O₅ nanowires with (0 1 0) twins were firstly discovered and synthesized using catalyst-free method by Tao and Li (2008). The Mg₂B₂O₅ nanowires were synthesized by applying NaCl/KCl flux method and the starting materials that are used are MgCl₂.6H₂O and H₃BO₃ as Magnesium and Boron source. The twinned Mg₂B₂O₅ nanowires were formed after calcining the mixture at 830°C for 2 hours. The microstructure and the mechanical properties of twinned Mg₂B₂O₅ nanowires were investigated by TEM and nano-indentation test, respectively.

As magnesium pyroborates have been widely used as an additive namely antiwear and anticorrosion additive (Došler et al., 2010). Mg₂B₂O₅ has prepared via two-step method included the co-precipitation hydrothermal technique of MgBO₂(OH) and thermally conversion of as-prepared MgBO₂(OH) to Mg₂B₂O₅ nanowhiskers at 650-700°C. The effects of temperature, heating procedure and rate on the thermal conversion of Mg₂B₂O₅ have been examined. It observed that, the physically absorbed water and structural water were eliminated at 470°C and 620°C, respectively and the high aspect ratio of nanowhiskers of the calcined products obtained by decreasing the heating rate and lower temperature. Whereas the low pores and high crystalline product are formed at higher temperature (Zhu et al., 2008).

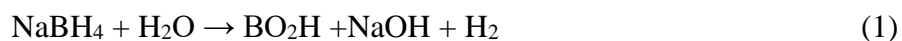
Solvothermal method was also used in the preparation of Mg₂B₂O₅. Both Triclinic Mg₂B₂O₅ and Orthorhombic Mg₂B₃O₆ have been synthesized by Xu et al (2008) under demanding conditions. MgCl₂, ethanol and NaBH₄ were used as the raw materials. The homogenized mixture was transferred into an autoclave and was heated for 6 hours at 400°C. The morphology, the phase of products and the effect of solvent were determined.

Single-phase magnesium pyroborates have also been successfully synthesized using solid state reaction method where MgO and 14% wt excess of B₂O₃ are used as the initial materials. The homogenized materials were heated for 10 hours at 600°C, 900°C, 1000°C, and 1200°C. The single-phase magnesium pyroborates were formed at 1200°C and 1250°C; both triclinic and monoclinic crystal phase were reported. The single phase Mg₂B₂O₅ was further characterized structurally and dielectrically (Doşler et al., 2010).

High temperature solid state reaction method has also been used for the preparation of magnesium pyroborate by (Üçyıldız and Girgin, 2010). In this synthesis process, the homogeneous mixture of MgO and H₃BO₃ were heated for an hour at temperature between 600-1050°C and it reported that monoclinic Mg₂B₂O₅ that is formed at 750°C is started to change slowly into triclinic Mg₂B₂O₅ as temperature increases and showed a significant change at 950°C. The best formations of monoclinic and triclinic Mg₂B₂O₅ were obtained after heating the prepared material for 4 hours at 850°C and 1050°C, respectively. Both chemical and physical properties of Mg₂B₂O₅ such as its chemical composition, surface area, particle size distribution have also been studied.

Single crystalline of monoclinic Mg₂B₂O₅ nanorods with width and length are 200 nm and 4-5 µm, respectively were acquired by another two-step method included mechano-chemical process and sintering process where the milled products of MgCl₂.6H₂O and NaBH₄ were sintered at 800°C for 2 hours. The physical properties of prepared products were characterized by XRD, TEM, EDS and also SAED (Li et al., 2010).

Afterwards, Li et al (2012) have also synthesized Mg₂B₂O₅ nanorods by using CTAB (cetyltrimethylammoniumbromide) as a soft template. The precursors were heated at 800°C for 2 hours and various molar ratio of Mg:B were applied. The formation of Mg₂B₂O₅ was followed as reaction below,



The crystal structure and morphology of thus prepared samples were characterized by XRD, SEM and also Raman spectrometer. The monoclinic phase

were observed and the best results were obtained with 1:4 molar ratio of Mg:B in the presence of CTAB.

Co-precipitation and sintering method were applied for the preparation of $\text{Mg}_2\text{B}_2\text{O}_5$. $\text{MgCl}_2 \cdot 6\text{H}_2\text{O}$, H_3BO_3 and NaOH were used as the initial materials. Also, KCl was used as a flux. The as prepared products were sintered at 655°C , 832°C and 988°C , respectively for 5 hours. It reported that monoclinic phase of $\text{Mg}_2\text{B}_2\text{O}_5$ were obtained at lower temperature whereas triclinic $\text{Mg}_2\text{B}_2\text{O}_5$ was obtained at higher temperature, 988°C . The morphology and the formation of $\text{Mg}_2\text{B}_2\text{O}_5$ were also discussed (Zhu et al., 2012)

Another method has also applied in the preparation of $\text{Mg}_2\text{B}_2\text{O}_5$ called Microwave energy method. The initial materials namely, MgO and H_3BO_3 were allowed to react in microwave furnace at 270W, 360W and 600W with time range 1-8 minutes. The properties of products such as its morphology and particle size of the products were characterized by using FT-IR, XRD, Raman Spectroscopy and SEM. The yields of the product thus prepared were also determined which found to be 67% at 270W and 360W in reaction times of 8 minutes and 3 minutes, respectively (Kipcak et al., 2013a).

In the same year, Kipcak et al. (2013b) also synthesized both dehydrated $\text{Mg}_3\text{B}_2\text{O}_6$ and $\text{Mg}_2\text{B}_2\text{O}_5$ via solid state method where their neutron shielding behavior was determined and compared. $\text{Mg}_2\text{B}_2\text{O}_5$ were prepared with 1:1 mole ratio at 800°C , 900°C and 1000°C . The yields of products and the neutron transmission value are 46-53% and 0.772-0.843, respectively. It observed that against neutron radiation dehydrated $\text{Mg}_3\text{B}_2\text{O}_6$ are better than dehydrated $\text{Mg}_2\text{B}_2\text{O}_5$ and has higher crystal score than $\text{Mg}_2\text{B}_2\text{O}_5$.

Zhu et al. (2014) have also synthesized $\text{Mg}_2\text{B}_2\text{O}_5$ nanowhiskers by noncorrosive, easy scale-up hydrothermal method by using MgCl_2 , H_3BO_3 , and NaOH as starting materials. Unlike their previous work, the precursors were milled in NaCl rich solution and surfactant poly(oxyethylene) 9 nonylphenol ether (NP-9) along the thermal conversion and then heated at 700°C for 2 hours with heating rate of $1.0\text{-}10^\circ\text{C}/\text{min}$. The pore-free $\text{Mg}_2\text{B}_2\text{O}_5$ nanowhiskers with high crystallinity were obtained.

Moreover, single crystalline $\text{Mg}_2\text{B}_2\text{O}_5$ nanowires that based on the post annealing of PVP-assisted were hydrothermally synthesized at a low temperature by using $\text{MgBO}_2(\text{OH})$ as precursors. In this study, $\text{Mg}_2\text{B}_2\text{O}_5$ was prepared by the thermal conversion of $\text{MgBO}_2(\text{OH})$ to $\text{Mg}_2\text{B}_2\text{O}_5$ caused dehydration and recrystallization process. It stated that at 600°C and 360°C , the elimination of structural water and physically absorbed water were observed, respectively. The processes were followed by the recrystallization process at 700°C . The mechanical strength of the as-prepared product was analyzed by applying it as an additive in PHA polymers to form composites. The addition of $\text{Mg}_2\text{B}_2\text{O}_5$ as additive to polymers increases the toughness and the rigidity of the composites (Mo et al., 2014).

The whiskers of $\text{Mg}_2\text{B}_2\text{O}_5$ were synthesized by in situ synthesis of porous ceramics with a framework structures. They were formed by using $[(\text{MgCO}_3)_4 \cdot \text{Mg}(\text{OH})_2 \cdot 5\text{H}_2\text{O}]$ or BMC, H_3BO_3 , and $\text{Ni}(\text{NO}_3)_2$ as raw materials. The physical properties of the product were investigated and compared by the absence and the presence of $\text{Ni}(\text{NO}_3)_2$. The materials mixtures were pre-sintered for an hour at 700°C and were heated at $800\text{-}1000^\circ\text{C}$ for 4 hours. The whiskers with diameter of $0.3\text{-}0.4\ \mu\text{m}$ and length of $2\text{-}5\ \mu\text{m}$ were acquired. it showed that, the monoclinic $\text{Mg}_2\text{B}_2\text{O}_5$ changed into triclinic $\text{Mg}_2\text{B}_2\text{O}_5$ by sintering at 900°C and the addition of $\text{Ni}(\text{NO}_3)_2$ increased the compressive strength of porous ceramics but decreased the diameter and length of the ceramics (Chen et al., 2014).

In 2015, an environmental friendly non-aqueous ionic liquid method has been successfully synthesized whiskers-like $\text{Mg}_2\text{B}_2\text{O}_5$ by heating the homogenized mixture of $\text{MgCl}_2 \cdot 6\text{H}_2\text{O}$, H_3BO_3 , NaCl and surfactant NP-9 at 850°C for 2 hours. The formation mechanism of whiskers-like $\text{Mg}_2\text{B}_2\text{O}_5$ and also the effect of non-aqueous ionic liquid on the morphology of the as-prepared products were determined (Liang et al., 2015).

Chiefly, the electrospinning technique was used for the preparation of $\text{Mg}_2\text{B}_2\text{O}_5$. Instead of nanorods, $\text{Mg}_2\text{B}_2\text{O}_5$ fibers were synthesized. MgO and 2-alkoxide were used as a starting material where N,N-dimethylformamide was also added for developing the fibrous structure. As the concentration of initial materials increases the thicker fibers of $\text{Mg}_2\text{B}_2\text{O}_5$ were observed. The crystalline fibers of $\text{Mg}_2\text{B}_2\text{O}_5$ were achieved by heating the samples at 1000°C with $\text{Mg}_3\text{B}_2\text{O}_6$ as by-

products. The morphology and crystal structures of the products were investigated (Storti et al., 2016).

Fan et al. (2017) have also synthesized $\text{Mg}_2\text{B}_2\text{O}_5$ ceramic by solid state reaction. Unlike the processes that have mentioned before, the mixture of starting materials were milled in alcohol using zirconium ball for 4hours, pressed into pellet after drying and mixed with 5% wt PVA. The $\text{Mg}_2\text{B}_2\text{O}_5$ that is sintered for 4 hours in air at 1000-1125°C were all in single phases, well densified after sintered at 1050°C and showed great microwave dielectric properties after sintered at 1100°C.

Recently, Zampiva et al. have synthesized $\text{Mg}_2\text{B}_2\text{O}_5$ in the atmosphere consisting of acetonitrile and hydrogen gas with a heat treatment at 1100°C. It reported that the atmosphere during the preparation plays an important role as under the Argon the mixture of $\text{Mg}_2\text{B}_2\text{O}_5$ and $\text{Mg}_3\text{B}_2\text{O}_6$ were observed and under hydrogen gas, $\text{Mg}_3\text{B}_2\text{O}_6$ was observed. Moreover, under Hydrogen gas together with acetonitrile $\text{Mg}_2\text{B}_2\text{O}_5$ was obtained (Zampiva et al., 2019).

Besides $\text{Mg}_2\text{B}_2\text{O}_5$, many magnesium pyroborates mixed metals have been synthesized in recent years. Fernandes et al (2004) have investigated the thermodynamic and magnetic properties of mixed metal pyroborate MnMgB_2O_5 . Although, Mn^{2+} ions have large magnetic moment, MnMgB_2O_5 found to be freeze in a glassy state at below 600 mK.

In 2010, the photoluminescence properties and crystal structure of manganese (II) doped magnesium pyroborates were investigated by Kawano et al. The solid solution of $\text{Mg}_2\text{B}_2\text{O}_5: \text{Mn}^{2+}$ was synthesized by another solid-state reaction method at 1000°C in argon by using MgO , MnO and H_3BO_3 as starting materials. The triclinic phase of $\text{Mg}_2\text{B}_2\text{O}_5: \text{Mn}^{2+}$ and a broad red emission at ~670 nm were observed (Kawano et al., 2010).

Mixed metal pyroborate MgFeB_2O_5 has also synthesized by solid state reaction method in order to investigate their suitability as Mg-ion battery cathode. Both Mg-rich and Fe-rich sample of MgFeB_2O_5 were prepared and analyzed. It reported that, at temperature around 250°C MgFeB_2O_5 transports Mg^{2+} ions (Bo et al., 2015).

MgMnB₂O₅ has been synthesized by ceramic method in 2017 by Glass et al., which the effects of composition on the performance of MgMnB₂O₅ were investigated. Furthermore, the change in the crystal structure and the cations ordering of the pyroborate were also studied.

1.3 SYNTHESIS METHOD OF BORATES

Around the turn of the century diverse array of methods have been applied for the preparation of ceramic powders. Obtaining highly pure and homogeneous powders becomes the purpose and main advantage of each method. For these reasons, preparative methods are classified into three categories namely, solid state method, solid-gas method and solution method.

1.3.1 Solid State Method

There are five methods that are categorized as solid state method such as Conventional ceramic method, alkali flux process, solid state combustion method, metallurgical route, and mechano-chemical method. Among these methods, conventional ceramic method is the most common synthetic method because the reactants react directly at high temperatures, which usually lead to thermodynamically stable product. Generally, the grinded powders of oxides, oxalate, carbonate, nitrate, sulfides, phosphates and other metals containing compounds are used as the starting materials which then heated at very high temperature with long reaction time. The reaction rate of in this method is depends on the rate of nucleation, surface area and rate of diffusion of ion (Rao and Biswas, 2015).

1.3.2 Solid Gas Method

Chemical vapor decomposition is one of examples of Solid gas method. Chemical vapor decomposition or CVD is used widely in the preparation of ceramic nanopowders such as carbide, nitride and oxide nanopowders. CVD also used to

fabricate bulk materials and composites. Chemical reaction of this method occurs in the gas phase where the substrate is formed by the decomposition of thin solid film which generally takes place at $\sim 1000^{\circ}\text{C}$. In this method, gases such as CH_3SiCl_3 and H_2 are used as precursor gas and inert gas namely, Ar is used as a diluents gas (Xu et al., 2011; Yongdong and Yan, 2010).

1.3.3 Solution Method

Solution methods have been used frequently due to their fascinating characteristics that lead to high purity powder with fine particle size. It consisted of three methods which are sol-gel process, co-precipitation technique and solution combustion method. In sol-gel process, the reactants such as alkoxides, acetates, formates or acetylacetonates are hydrolyzed and polycondensated in organic solvents to form polymeric gels and forming the products after calcining at certain temperature. In co-precipitation method, carbonates and nitrate usually used as starting materials. In this method, the metal salts are precipitated as hydroxides, oxalates or carbonates in the presence of precipitating agents followed by washing, drying and heating to obtain the final product (Xu et al., 2011).

1.3.3.1 Solution Combustion Synthesis (SCS)

Solution combustion method was firstly presented as a high temperature synthesis known as combustion synthesis by Merzhano et al in 1967. Due to its spontaneous combustion, this method produces a highly exothermic reaction between reactants and flame and become self-sustaining as the reaction takes place. However, it is upgraded by Patil et al into Solution combustion synthesis by combining with a wet chemistry due to its large size particle and difficult to access. Solution combustion synthesis or SCS is a versatile method that has received much interest due to its ability to synthesize nanoscale materials in a controlled size and composition based on the exothermicity of redox reaction. SCS makes use of metal salts such as nitrates, carbonates and sulfates as oxidizing agent (oxidant) and fuels such as glycine, urea, sucrose, starch and other water soluble carbohydrate as a

reducing agent. These days, SCS is used mostly in the preparation of metals, metal oxides, metal borates, metal sulfides, metal phosphates, metal silicates and alloys. Furthermore, SCS is also recognized by its time and energy efficiency as it is an auto-propagated process by self-sustained combustion reaction.

Moreover, there are some other advantages of solution combustion method as follows;

- i. Relatively simple and low cost, also solution combustion synthesis suitable for scale-up production.
- ii. Produce high quality product with variety of structures such as metal-matrix composites, metallic, carbides, nitrides, ceramics, oxides and many more.
- iii. Synthesis the high purity product of ternary and quaternary oxides.
- iv. Forming metastable phase in a short time which leads to novel performance achievement.
- v. In the case of photocatalysts, solution combustion synthesis can produce a product with high active surface area (Li et al., 2015; Rao and Biswas, 2015).

The reaction mechanism of solution combustion process is depends on many parameters such as fuels, oxidizer, fuel-oxidizer ratio, the amount of water used while mixing the starting materials and the ignited temperature. Surface area, morphology, phase, crystallite size, agglomeration and the particle and pore size of the final product can be affected by the ratio of fuel and oxidizer (Kopp Alves et al., 2013). The fuel quantity plays a very important role as it can affect the degree of crystallinity and physical properties of the product. The best fuels and oxidizer should have low decomposition temperature, high solubility in the solvent, low cost and readily available. Furthermore, for the fuels it should not yield residual mass and should not lead to explosion. Among various fuels and oxidizers, the most common ones are listed in Table 1.3.

Most ideal fuels for combustion synthesis are glycine and urea. In Addition, metal nitrate is the most frequently used oxidizer; not only because of it is a high efficiency oxidizing agent but also it high solubility in water (solvent) and low

decomposition temperature allow the formation of active oxygen which lead to a high solution concentration. In this Synthesis, the solution containing oxidizer and fuel dissolve in solvent is started to react by heating at certain temperature. It starts with the hydration of solvent and decomposition of gel follows by self-ignited of the gel which then burns and forms the final product. Generally, the solution is heated at temperatures between 300-500°C (Li et al., 2015; Varma et al., 2016).

Table 1.3. The Most Common Used Starting Materials in SCS

Oxidizer	Metal nitrate or metal hydrate ($M^x(NO_3)_x \cdot nH_2O$)
	Ammonium nitrate (NH_4NO_3)
	Nitric acid (HNO_3)
Fuel	Acetylacetone ($C_5H_8O_2$)
	Carbohydrazide (CH_6N_4O)
	Citric acid ($C_6H_8O_7$)
	Glucose($C_6H_{12}O_6$)
	Glycine ($C_2H_5NO_2$)
	Hexamethylenetetramine ($C_6H_{12}N_4$)
	Oxalyldihydrazide ($C_2H_6N_4O_2$)
	Sucrose ($C_{12}H_{22}O_{11}$)
	Urea (CH_4N_2O)
Solvent	2-methoxyethanol ($C_3H_8O_2$)
	Benzene (C_6H_6)
	Ethanol (C_2H_6O)
	Formaldehyde (CH_2O)
	Furfuryl alcohol ($C_5H_6O_2$)
	Kerosen
	Methanol (CH_4O)
	Water (H_2O)

The fuel and oxidizer ratio is determined on the basis of propellant chemistry where the valences of both fuel and oxidizer are under consideration. Valence of oxidizing and reducing element are negative and positive, respectively. The reducing element such as Carbon, Hydrogen, Boron are having valences of +4,+1,+3, respectively and Oxygen which is considered as oxidizing element with valence of -2. Furthermore, due to its conversion into the molar nitrogen in combustion reaction, nitrogen's valence is zero (Sambandan, 2008).

In recent years, some studies have done for the preparation of $Mg_2B_2O_5$ by solution combustion method. Altuntaş Öztaş and Erdoğan have synthesized $Mg_2B_2O_5$ by using two different methods such as solution combustion synthesis and conventional ceramic process. The results obtained from each method were compared and analyzed. In solution combustion method, $Mg(NO_3)_2 \cdot 6H_2O$, H_3BO_3 as oxidizer and carbonylhydrazide as fuel. The homogenous mixtures introduced to furnace at $400^\circ C$ for 5 minutes. Various Fuel-Oxidizer ratios were also tried and it reported that the morphologies, surface area and pore size are changed as ratio changed. The best results with high crystallinity were determined when 1.25:1 of B: Mg is used and the fuel-oxidizer ratio between range of 0.7: 1 to 1:1 (10%, 20% and 30% of fuel excess in quantity). Single phase of triclinic $Mg_2B_2O_5$ were achieved (Altuntaş Öztaş and Erdoğan, 2009).

Submicron rods of $Mg_2B_2O_5$ has been prepared by solution combustion methods which $Mg_2(NO_3)_2 \cdot 6H_2O$, H_3BO_3 , glycine and carbamide were used as starting materials with molar ratio 1:1 of Mg:B. The materials were heated in the furnace at $900^\circ C$ followed by calcinations for 4 hours. The crystal structure and morphology of products were characterized by XRD, SEM, and TG-DTA. The diameter distributes was examined to be in the range of 200 nm to 400 nm. Also, the ratio of length and diameter distributes are observed to be from 3 to 6 (Jia et al., 2015).

2. AIM AND SCOPE OF THE STUDY

The main purpose of this study is to synthesize and characterize pure magnesium pyroborates by the easier and simpler method: solution combustion synthesis. The reaction conditions were varied by using different organic fuels (carbohydrazide, citric acid, glycine, HMDA, HMTA, tartaric acid and urea) and heating temperature to examine their effects on the crystal structures, crystallite sizes and optical band gap energy, comparatively.



3. MATERIALS AND METHODS

3.1 CHEMICALS

In this present work, the chemicals that were used are listed as follows;

Magnesium nitrate hexahydrate, $\text{Mg}(\text{NO}_3)_2 \cdot 6\text{H}_2\text{O}$: Merck, 99.00%

Boric acid, H_3BO_3 : Merck, 99.00%

Carbohydrazide, CON_4H_6 : Aldrich, 98.00%

Citric acid monohydrate, $\text{C}_6\text{H}_8\text{O}_7 \cdot \text{H}_2\text{O}$: Merck, 99.50%

Glycine, $\text{C}_2\text{H}_5\text{NO}_2$: Merck, 99.70%

Hexamethylenediamine (HMDA), $\text{C}_6\text{H}_{16}\text{N}_2$: Merck, 99.00%

Hexamethylenetetramine (HMTA), $\text{C}_6\text{H}_{12}\text{N}_4$: 99.90%

Tartaric acid, $\text{C}_4\text{H}_6\text{O}_6$: Merck, 99.00%

Urea, $\text{CH}_4\text{N}_2\text{O}$: Merck, 99.50%

Potassium Bromide, KBr, for IR Spectroscopy: Merck, 99.90%

3.2 INSTRUMENTS

3.2.1 Fourier Transform Infrared Spectrophotometer

Infrared spectra of the final products were recorded by Shimadzu Fourier Transform Infrared (FTIR) spectrophotometer in the region of 4000-400 cm^{-1} . The spectra of the product was obtained by preparing the pellets that are consisted of 0.0010:0.1500(wt/wt) of KBr:product ratio.

3.2.2 X-ray Powder Diffractometer

Rigakuminiflex and multiflex X-ray powder diffractometer were used to provide the structural properties of product using $\text{CuK}\alpha$ (30-40kV, 10-20mA, $\lambda=1,54056 \text{ \AA}$) radiation. The data of each XRD patterns were obtained by using Rigaku programs and were checked by using ICDD data card.

3.2.3 UV- VIS Spectrometer

Perkin Elmer Lambda 35 UV-VIS Spectroscopy was used to determine the optical properties of the samples. The spectra were recorded at wavelength range of 200-900 nm. The data was plotted by using Data Processor WinLab.

3.2.4 Furnace

The reactions during the preparation of metal borates were carried out at heating range between 400-900°C by the aid of Nuve MF 120 furnace.

3.3 METHODS

Magnesium pyroborates ($\text{Mg}_2\text{B}_2\text{O}_5$) were synthesized by Solution Combustion Synthesis (SCS) using $\text{Mg}(\text{NO}_3)_2 \cdot 6\text{H}_2\text{O}$, H_3BO_3 and fuels starting materials. $\text{Mg}(\text{NO}_3)_2 \cdot 6\text{H}_2\text{O}$ and H_3BO_3 were used as Mg and B source, respectively with 1:1.05 of Mg:B mole ratio. Various fuels were also used in this synthesis such as carbohydrazide, citric acid, glycine, HMDA, HMTA, tartaric acid and urea.

3.3.1 Synthesis of Magnesium Pyroborates

Stoichiometric amount of $\text{Mg}(\text{NO}_3)_2 \cdot 6\text{H}_2\text{O}$, H_3BO_3 and fuel were dissolved in distilled water and 5wt% excess H_3BO_3 was applied. The homogeneous mixture was mixed using magnetic stirrer and was allowed to evaporate at 370°C until the gel-like residue was observed. Small amount of precursor-gel was collected for further thermal analysis and then the precursor-gel was introduced in a furnace preheated at 400°C for 5minutes. The as-prepared product was ground and the heating process was done at various temperatures in range between 400°C - 1000°C for an hour. All the heated products at each temperature were kept for characterization studies.

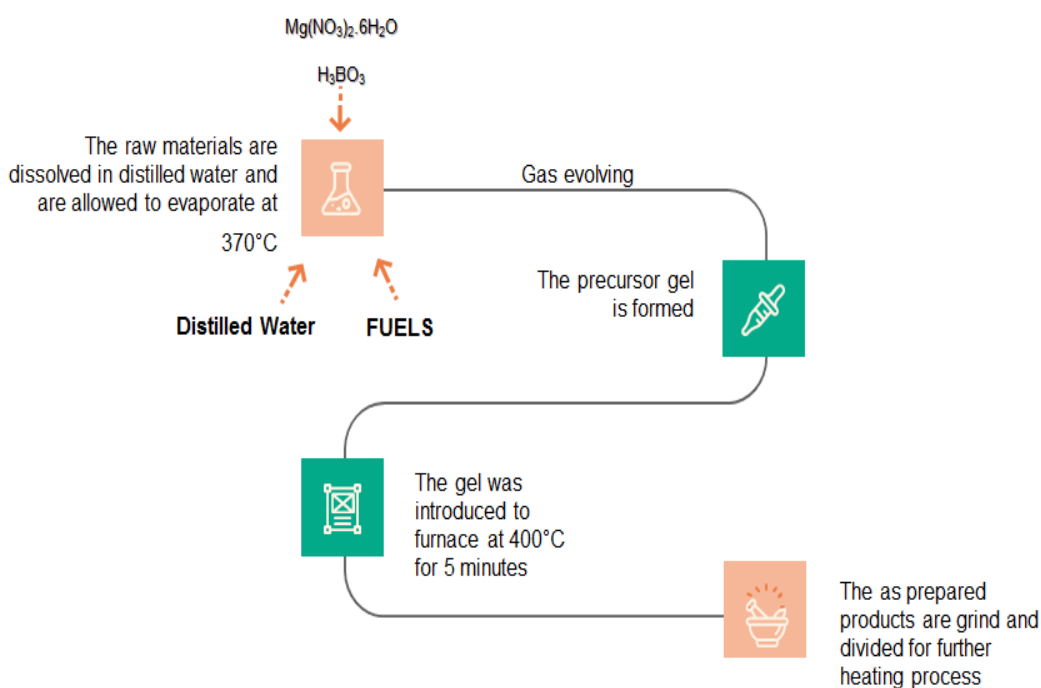
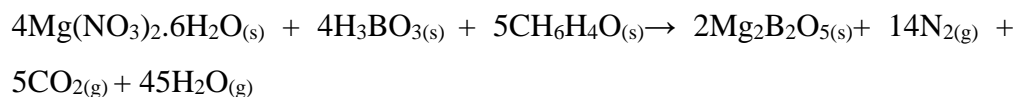


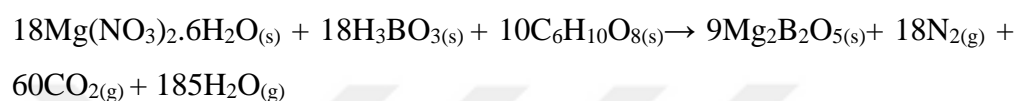
Figure 3.1. Schematic Diagram of $\text{Mg}_2\text{B}_2\text{O}_5$ Synthesis

The procedure above was applied to all fuels such as carbonylhydrazide, citric acid, glycine, HMDA, HMTA, tartaric acid and urea. The theoretical reaction of each fuels are described as follows;

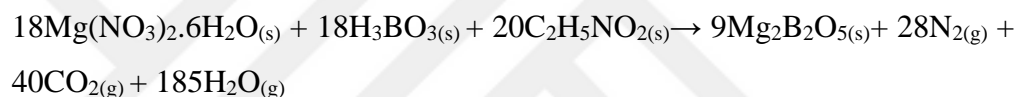
➤ **Carbonylhydrazide**



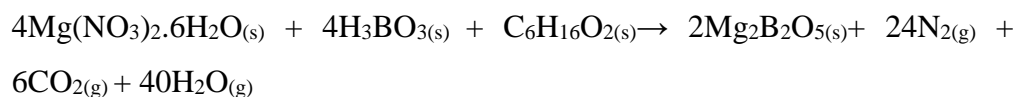
➤ **Citric Acid**



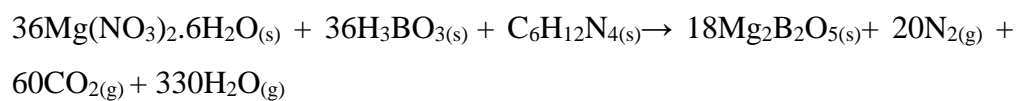
➤ **Glycine**



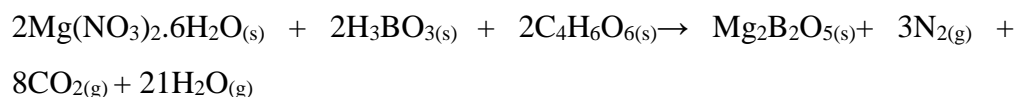
➤ **HMDA**



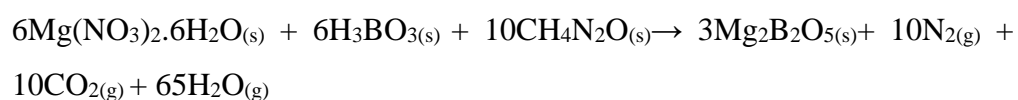
➤ **HMTA**



➤ **Tartaric Acid**



➤ **Urea**




4. RESULTS AND DISCUSSION





4.1 Synthesis of Pure Magnesium Pyroborates


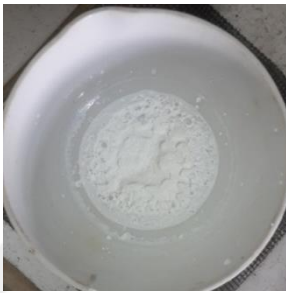
Magnesium pyroborates, $Mg_2B_2O_5$ were synthesized via Solution Combustion Synthesis (SCS) by adjusting the fuel types and temperatures. In order to examine its fuel effect, carbohydrazide, citric acid, glycine, HMDA, HMTA, tartaric acid and urea were used. Furthermore, reaction temperatures were also varied from $400^\circ C$ to $1000^\circ C$ and the samples were heated for an hour. Fuel:oxidizer ratio and Mg:B ratio were applied in 1:1 and 1: 1.05 mole ratio, respectively.

During the preparation of $Mg_2B_2O_5$, different behavior of solution was observed. Some fuels dissolved quickly in solvent, evolve more gases during synthesis or even produce different color and texture of powder after preheated process. The details of them were listed in Table 4.1.

Table 4.1. Observation during the Preparation of Pure $Mg_2B_2O_5$

Fuels	Observation	Picture
Carbohydrazide	The homogenized solution was colorless and produced colorless gel at $370^\circ C$. Moderate amount of gas evolves was observed. The as prepared product was hard and white color after preheated at $400^\circ C$ for 5mins. Small amount of product were obtained.	

Citric Acid	<p>The homogenized solution was colorless and produced a light yellow gel at 370°C. The amount of gas evolve was high and yellow gas was evolved when precursor-gel started to form. The product was fluffy and light cream in color after preheated at 400°C for 5mins.</p>	
Glycine	<p>The homogenized solution was colorless and produced a little amount of gas during the gel formation at 370°C. The precursor-gel was colorless and formed a fluffy light grey product after preheated at 400°C for 5minutes.</p>	
HMDA	<p>The homogenous solution was greenish in color and formed yellow-like gel at 370°C. The amount of gas evolved was very high. A fluffy soft product was obtained after preheated for 5 minutes at 400°C.</p>	
HMTA	<p>The gas evolves of the colorless solution was moderate, the light-yellow gel was observed at 370°C and after preheated at 400°C for 5 minutes, the white product was stuck in the evaporating dish and little bit hard.</p>	

Tartaric acid	The homogenous solution was colorless and formed yellow-like gel at 370°C. Moderate amount of gas evolved was observed. A fluffy soft product was obtained after preheated for 5 minutes at 400°C.	
Urea	The homogenous solution was cloudy and formed colorless gel at 370°C. The amount of gas evolved was moderate. A white hard product obtained after preheated for 5 minutes at 400°C.	

The products that obtained after the preheated process at 400°C for 5 minutes (synthesis) were heated at higher temperatures in the range between 400°C to 1000°C for an hour. The colors' changed of the products were observed depend on the fuels and the temperature applied. For the products that attained by using carbonylhydrazide as fuel, no color changed were observed. Although small amount of products were obtained, the color changes of products are can be observed because they are remain white in color at each temperature as shown in Figure 4.1.

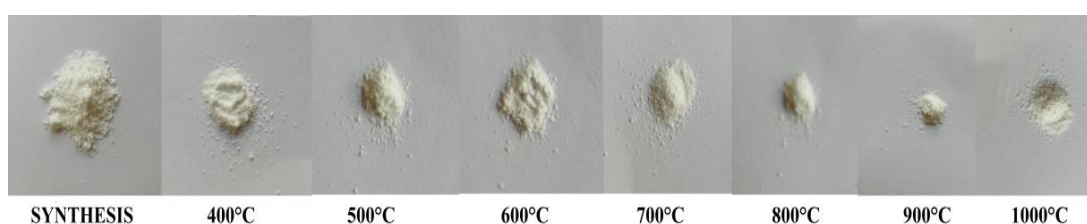


Figure 4.1. Digital Photos of $Mg_2B_2O_5$ with Carbonylhydrazide as Fuel

On the other hand, the products that obtained by using citric acid as the fuel showed a great color changes where the color become lighter from light brown to white with increasing temperatures (Figure 4.2).



Figure 4.2. Digital Photos of $Mg_2B_2O_5$ with Citric Acid as Fuel

Given in Figure 4.3, The synthesis products of $Mg_2B_2O_5$ with glycine fuel were also heated at higher temperature and it observed that the color of the products are getting light and lighter which the light grey color are slowly turned into white color as temperature increases.

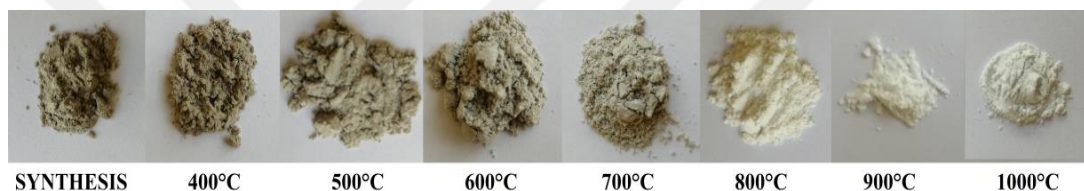


Figure 4.3. Digital Photos of $Mg_2B_2O_5$ with Glycine as Fuel

Unlike the products of $Mg_2B_2O_5$ with glycine fuel with grey synthesis products, the synthesis products that obtained by using HMDA fuels are light brown in color which then gradually change into a lighter color with increases in temperatures as shown in Figure 4.4.

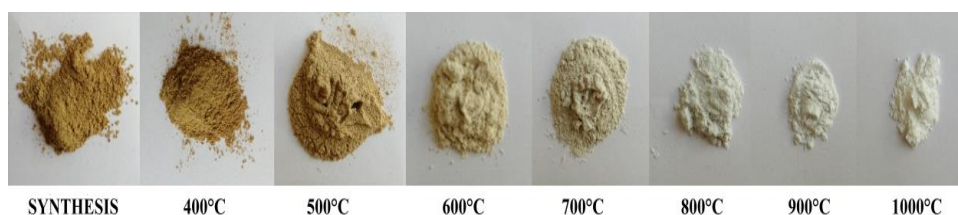


Figure 4.4. Digital Photos of $Mg_2B_2O_5$ with HMDA as Fuel

Similar to the behavior of products obtained by using carbonylhydrazide fuel, the products of $Mg_2B_2O_5$ with HMTA and urea showed no changed in color as temperature getting higher.

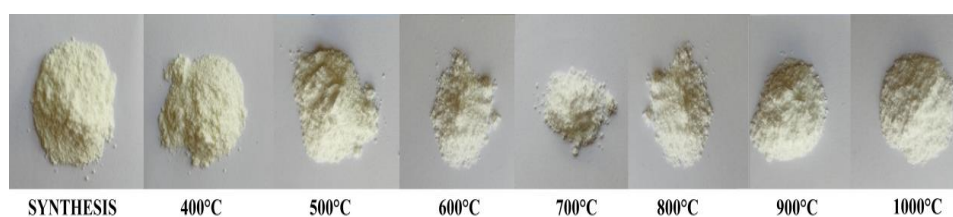


Figure 4.5. Digital Photos of $Mg_2B_2O_5$ with HMTA as Fuel

The color are remain in light cream color for the products obtained by HMTA fuel (Figure 4.5) whereas, white color products stay unchanged for the products formed by using urea as fuel (Figure 4.6).



Figure 4.6. Digital Photos of $Mg_2B_2O_5$ with Urea as Fuel

The products of $Mg_2B_2O_5$ with tartaric acid fuels show a very great alteration in color as it became darker at 500°C and turned into white color at 1000°C (Figure 4.7).

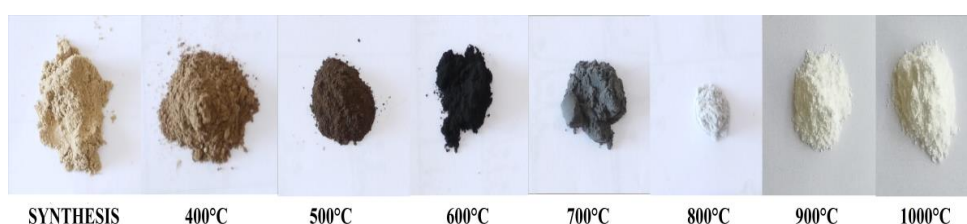


Figure 4.7. Digital Photos of $Mg_2B_2O_5$ with Tartaric Acid as Fuel

These behaviors of the products approved the fuels effects and the temperature effects on the physical properties of magnesium pyroborates. Moreover, these results also confirmed the color of magnesium pyroborate is white at the highest heating temperature despite the fuels are different.

4.1.1 Structural Characterization Studies of Pure $Mg_2B_2O_5$

4.1.1.1 FT-IR Spectroscopy Studies

The as-prepared products were firstly characterized by FT-IR spectroscopy where the spectra of each fuel at all temperatures were collected. The sharp peaks around 840cm^{-1} and 1026cm^{-1} indicate the B-O stretching vibrations of four coordinate boron of BO_4 , while the peak at 497cm^{-1} ascribed to the B-O-B bending of BO_4 . The band at about 1498cm^{-1} was observed due to the B-O asymmetric stretching of BO_3 . Meanwhile, the two bands at around 1292 cm^{-1} and 1170 cm^{-1} related to the stretching vibration of BO_3 . In more addition, the B-O-B bending of BO_3 was observed at 720 cm^{-1} and 682 cm^{-1} (Altuntaş Öztaş and Erdoğan, 2009; Karakassides et al., 1996; Storti et al., 2016; Weir and Schroeder, 1964).

Figure 4.8 presents the preheated products of $Mg_2B_2O_5$ at 400°C for 5 minutes. It observed that only carbohydrazide and glycine fuels formed magnesium pyroborates while the other fuels shown a board band around 1500cm^{-1} which due to the uncompleted reaction with boric acid. The board and strong band was also detected at about $2800\text{-}3600\text{ cm}^{-1}$ which represent the $-\text{OH}$ group stretching vibration boric acid. Although the products obtained by using other fuels are not as perfect as the spectra that formed by carbohydrazide and glycine fuel, it clearly showed that the vibrational bands of $Mg_2B_2O_5$ are do existed in their FT-IR spectra. After heating for an hour at 400°C and 500°C , it is observed that there are not much changed in FT-IR spectra was attained as shown in Figure 4.9 and 4.10, respectively.

Given in Figure 4.11, all the vibration bands of $Mg_2B_2O_5$ were started to form at 600°C for all fuels, except for the products that were obtained by citric acid and tartaric acid fuel which formed at 700°C (Figure 4.12). Furthermore, the spectra of products showed very identical bands with magnesium pyroborate bands that also viable in the spectra of the products obtained at 800°C and 900°C (Figure 4.13 and 4.14, respectively). It also resulted that the intensities of the bands increase along with temperature.

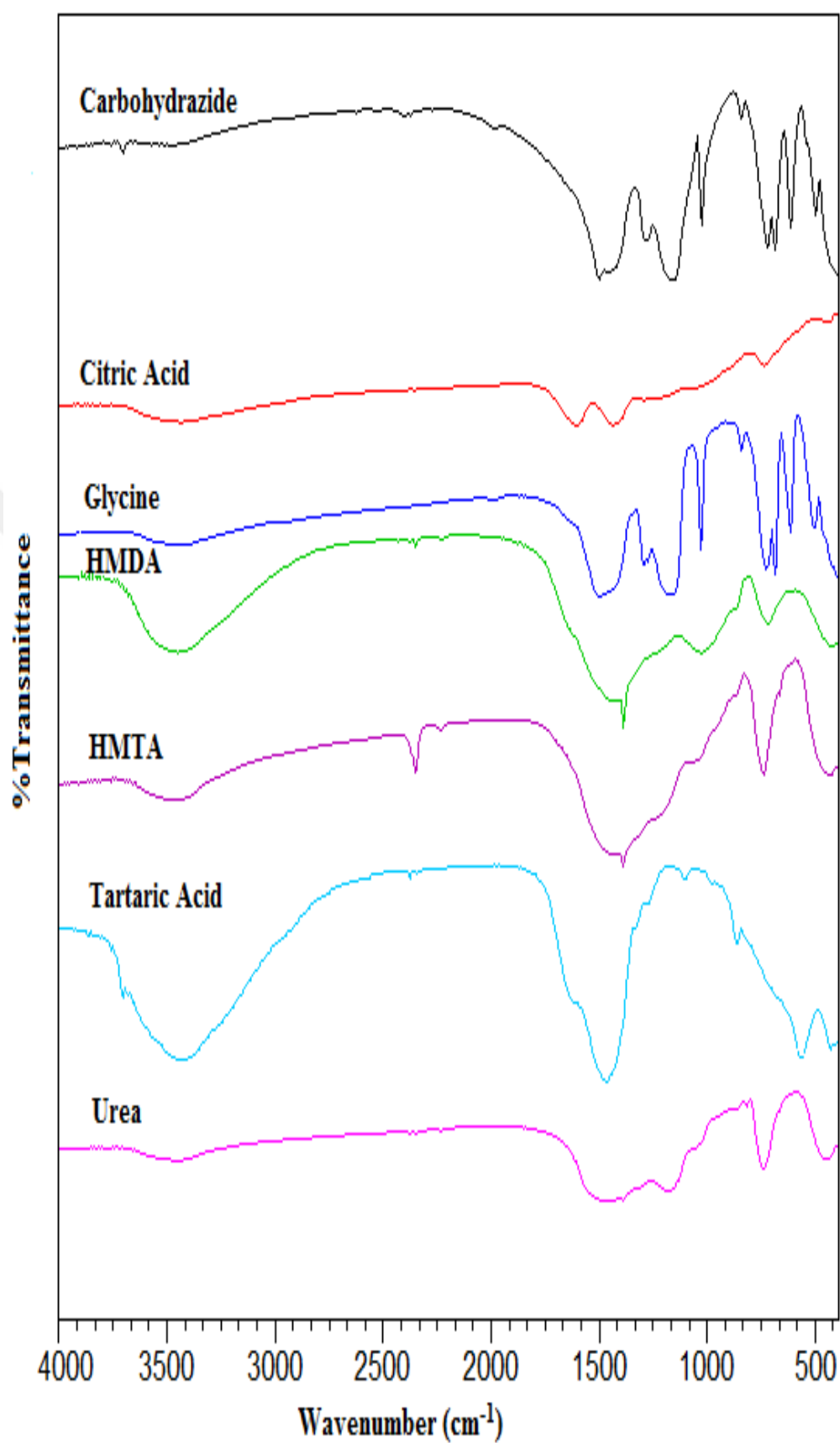


Figure 4.8. FT-IR Spectra of Synthesis $Mg_2B_2O_5$ Using All Fuels

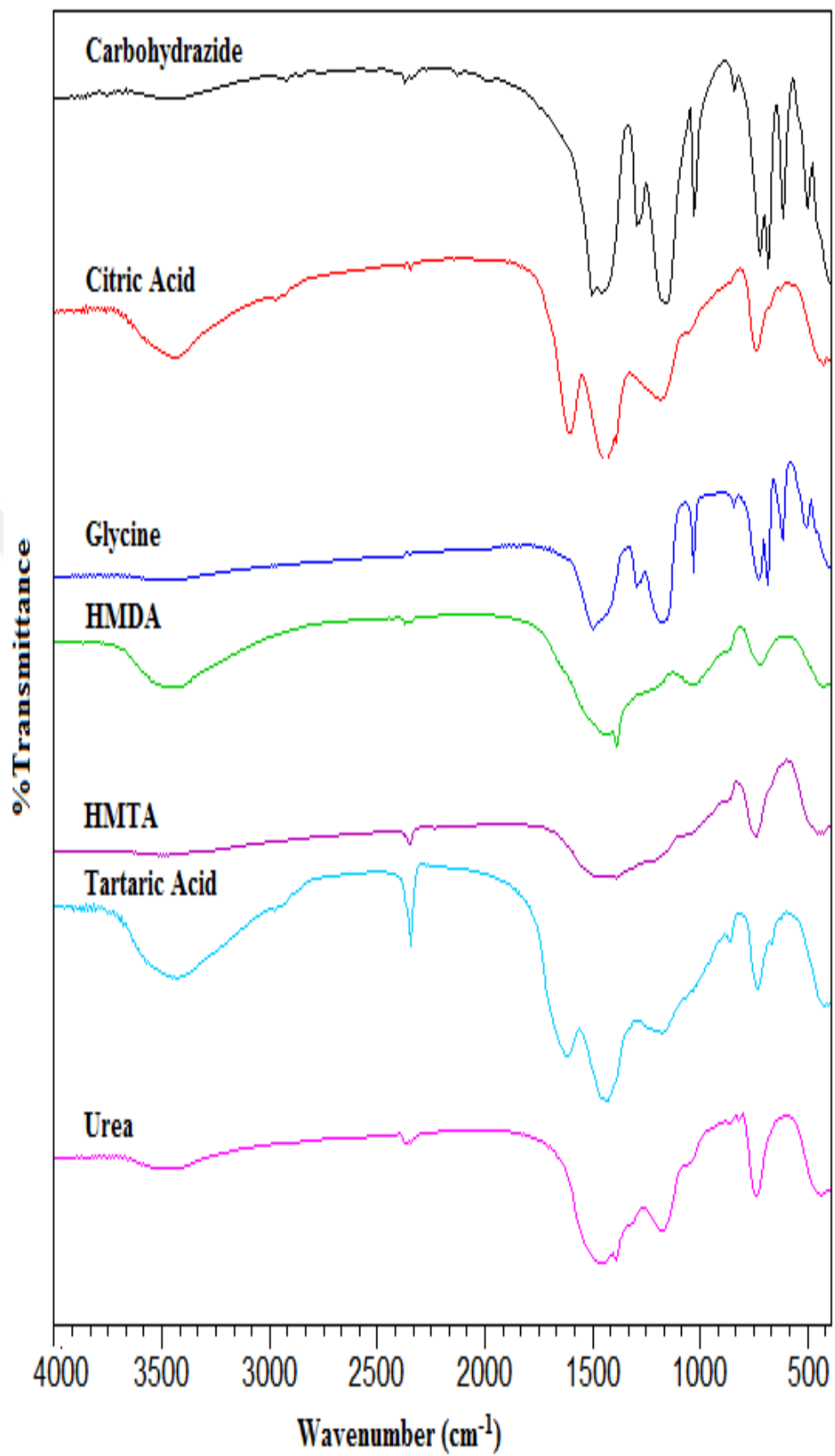


Figure 4.9. FT-IR Spectra of $Mg_2B_2O_5$ at $400^\circ C$ Using All Fuels

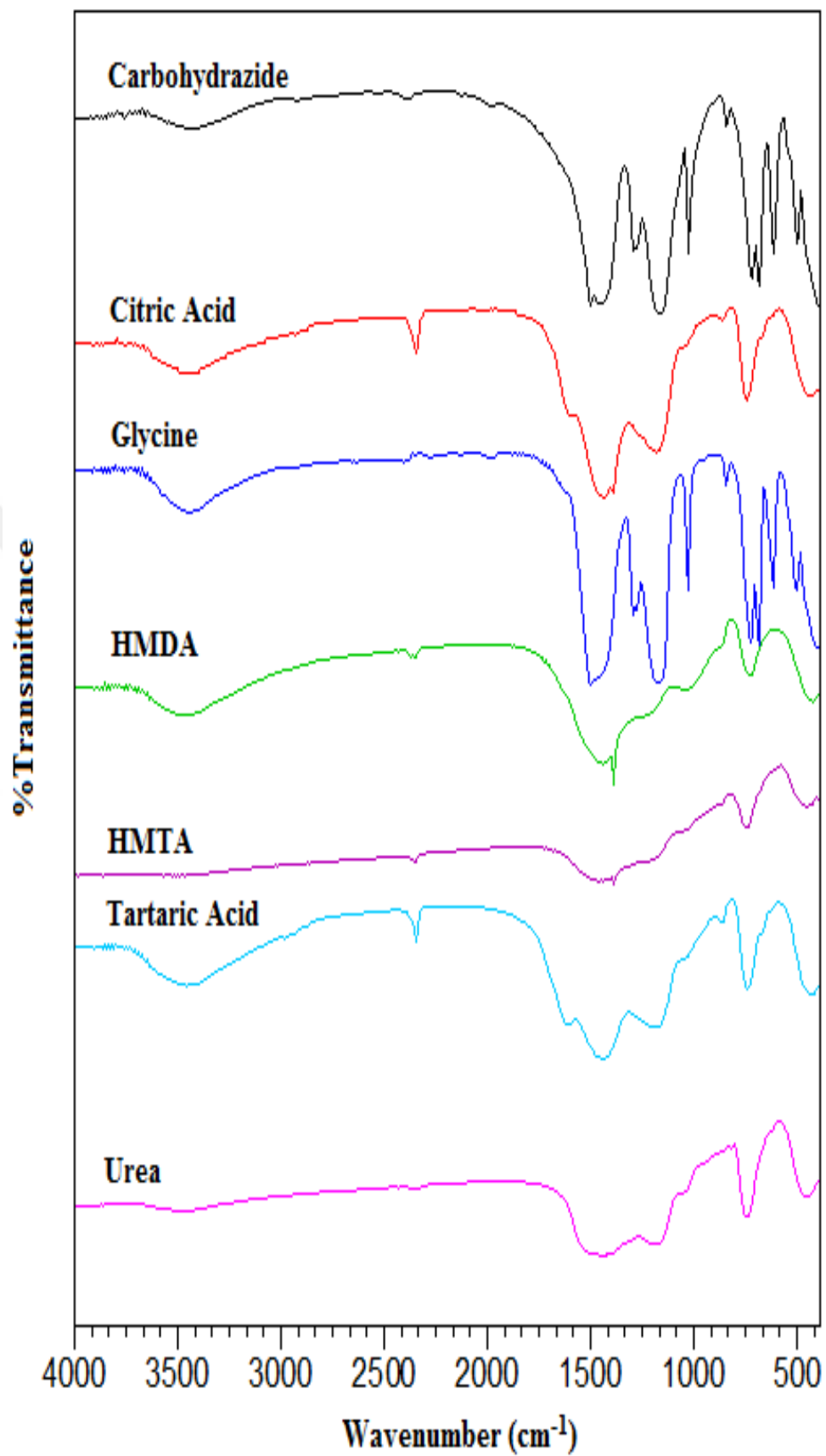


Figure 4.10. FT-IR Spectra of $Mg_2B_2O_5$ at $500^\circ C$ Using All Fuels

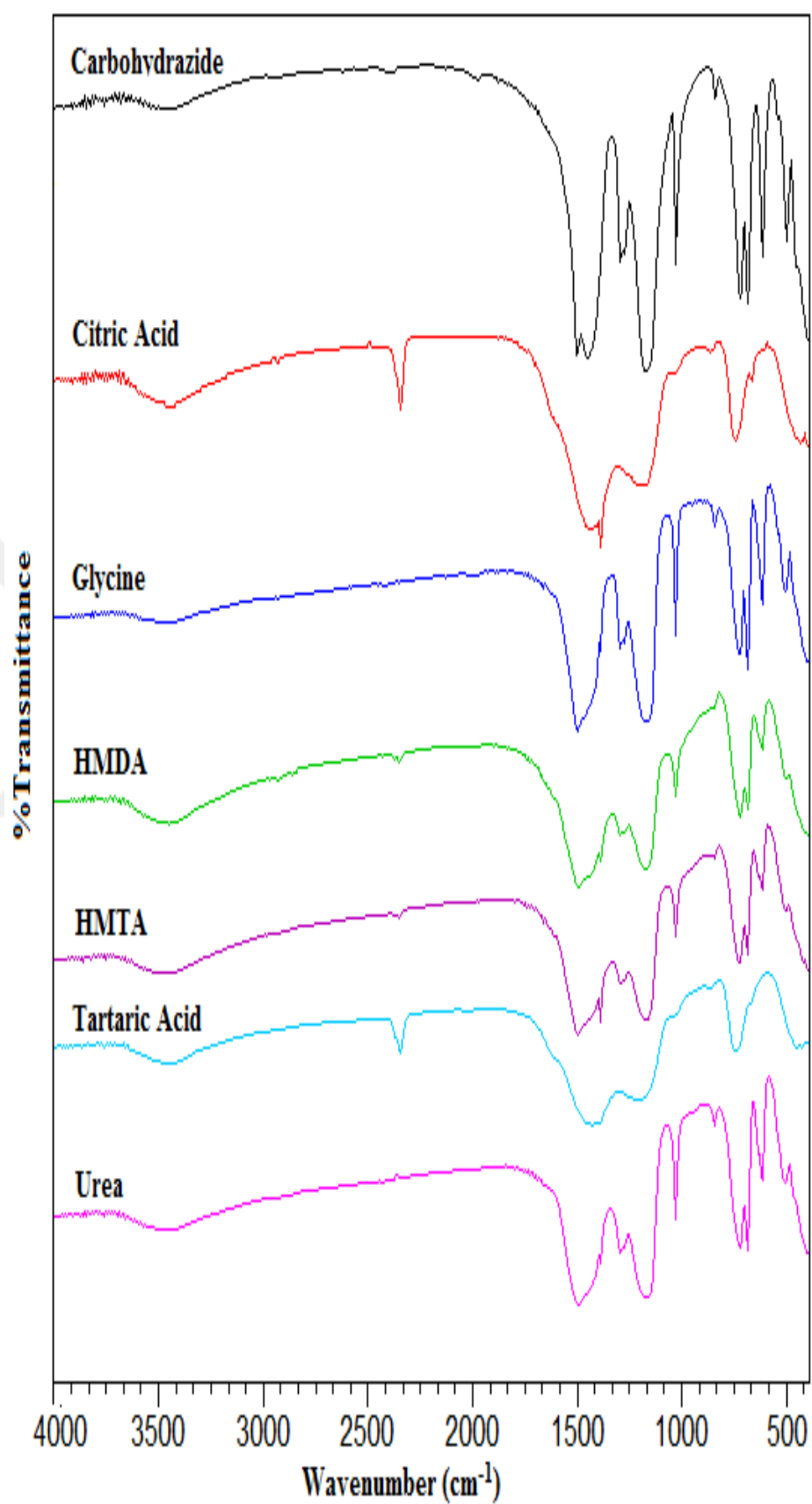


Figure 4.11. FT-IR Spectra of $Mg_2B_2O_5$ at $600^\circ C$ Using All Fuels

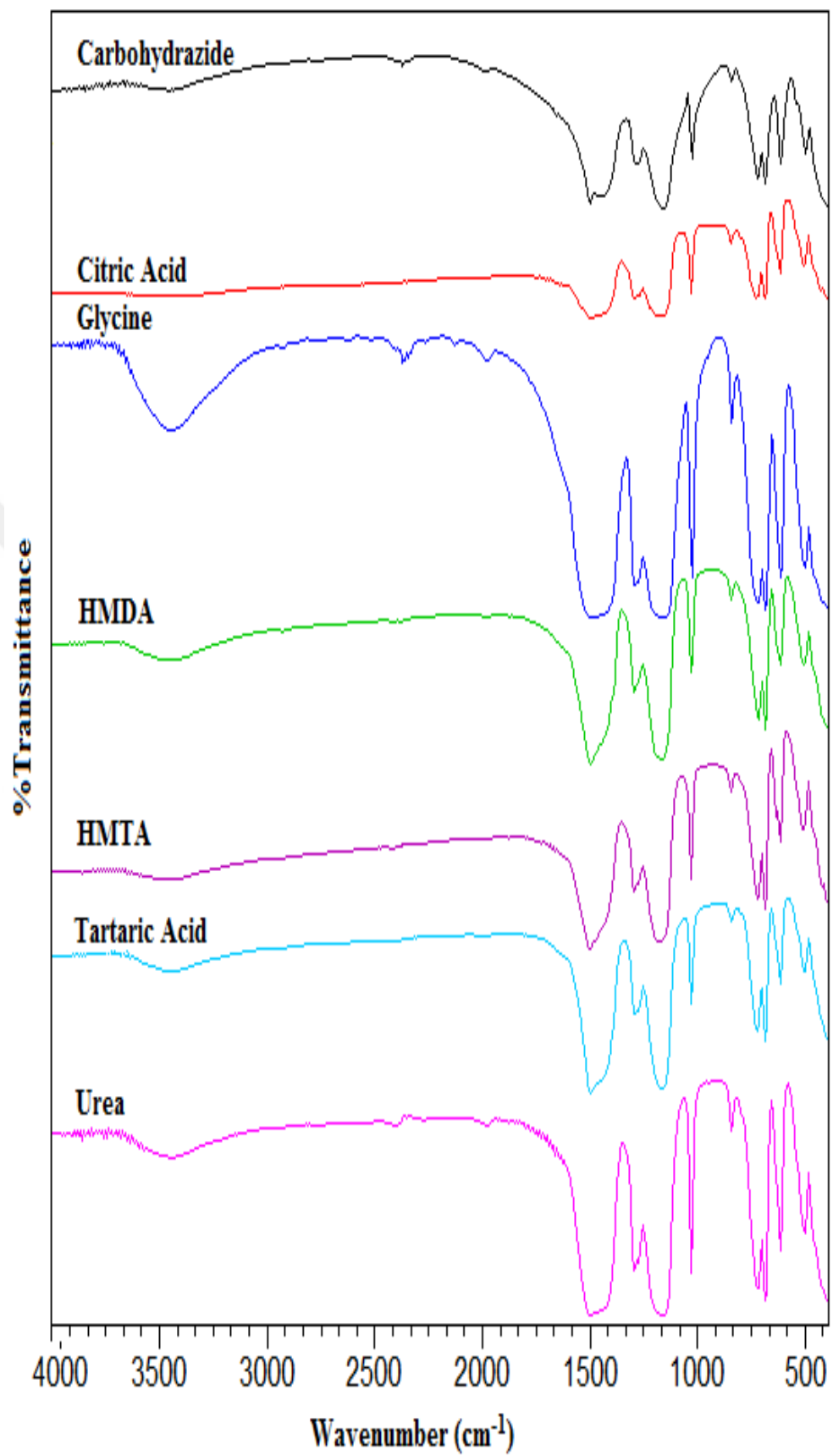


Figure 4.12. FT-IR Spectra of $Mg_2B_2O_5$ at $700^\circ C$ Using All Fuels

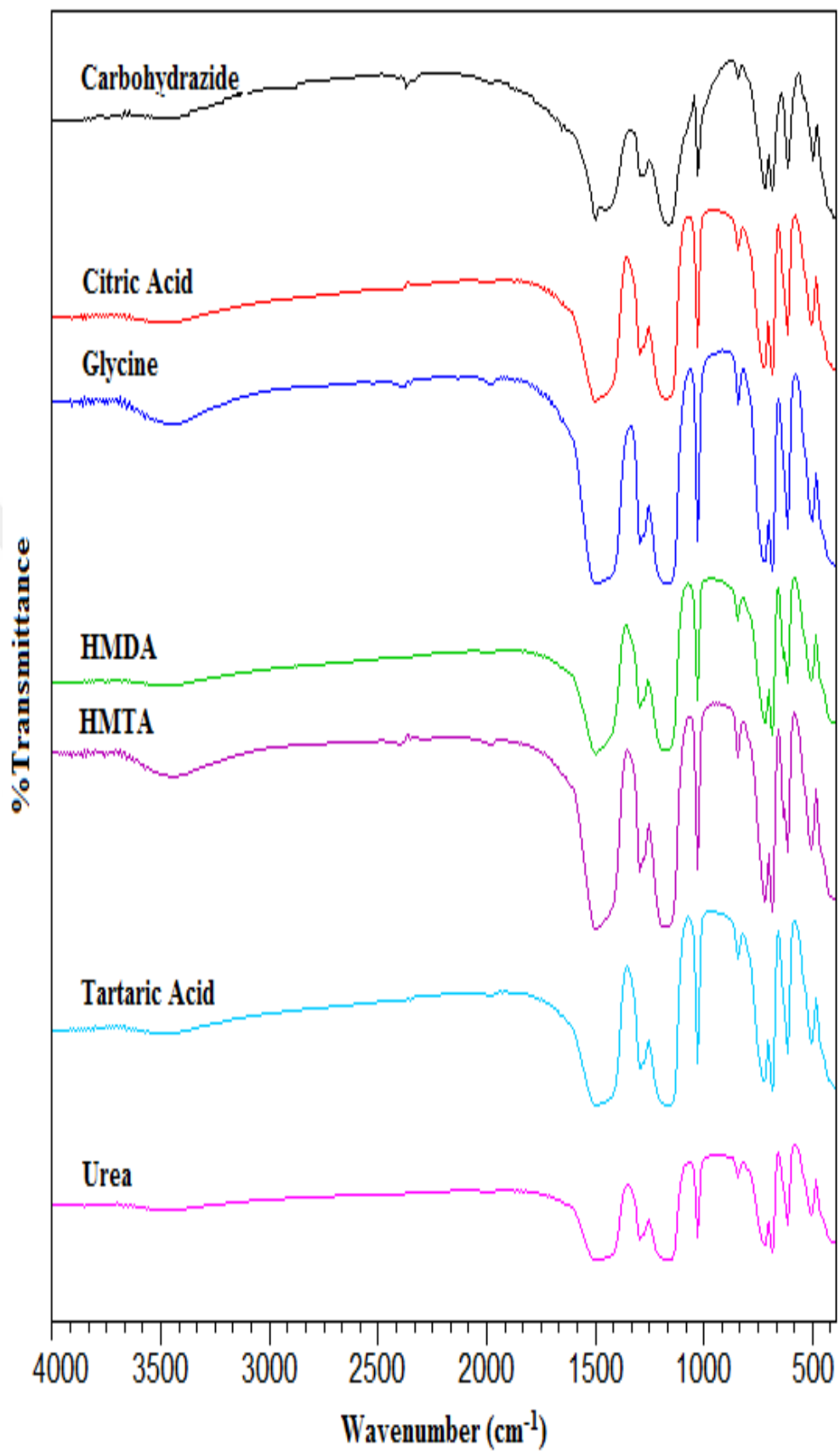


Figure 4.13. FT-IR Spectra of $Mg_2B_2O_5$ at $800^\circ C$ Using All Fuels

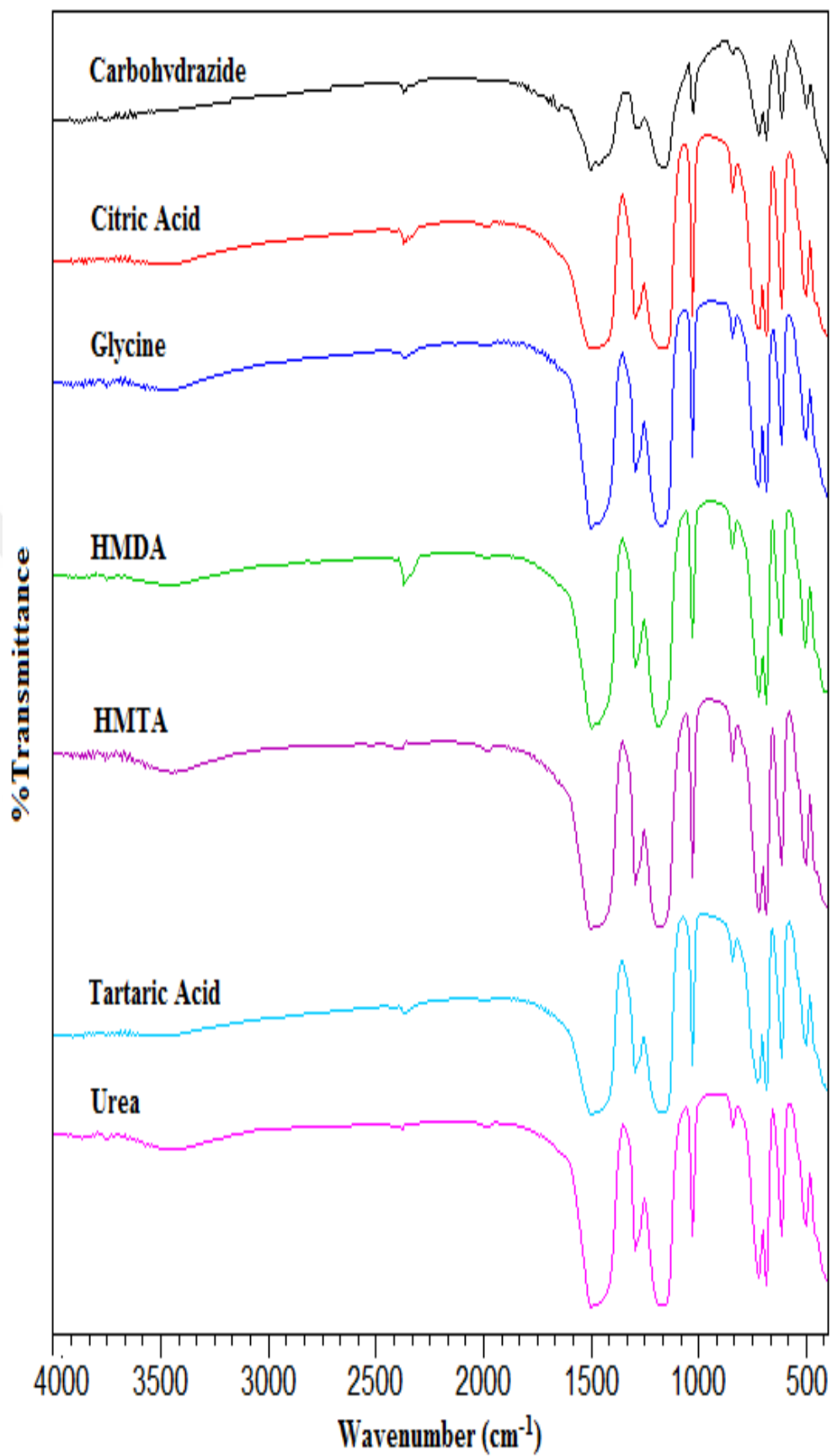


Figure 4.14. FT-IR Spectra of $Mg_2B_2O_5$ at $900^\circ C$ Using All Fuels

The excellent results with high crystallinity and zero impurities of all products were achieved at 1000°C. All the vibrational bands that were mentioned previously are shown in Table 4.2.

Table 4.2. FTIR Assignment of Mg₂B₂O₅ with all fuels and wavenumbers (cm⁻¹) at 1000°C

Mg ₂ B ₂ O ₅	Assignment		
	$\tilde{\nu}_1(\text{BO}_3)$	$\tilde{\nu}_2(\text{BO}_4)$	$\tilde{\nu}_3(\text{BO}_3)$
Carbohydrazide	681, 716	837, 1024	1163, 1290, 1497
Citric Acid	683, 718	837, 1026	1175, 1292, 1499
Glycine	683, 718	837, 1026	1177, 1292, 1497
HMDA	685, 718	839, 1026	1184, 1292, 1499
HMTA	683, 716	839, 1026	1182, 1292, 1495
Tartaric Acid	683, 718	837, 1026	1173, 1290, 1499

Given in Figure 4.15, the bands around 680 cm⁻¹ and 720 cm⁻¹ represent to the B-O-B bending of trigonal BO₃. The stretching vibration of trigonal BO₃ were observed at 1175 cm⁻¹, 1290 cm⁻¹ and 1490 cm⁻¹. Whereas, the stretching vibration of BO₄ assigns at about 837 cm⁻¹, 1026 cm⁻¹. No additional peaks were detected.

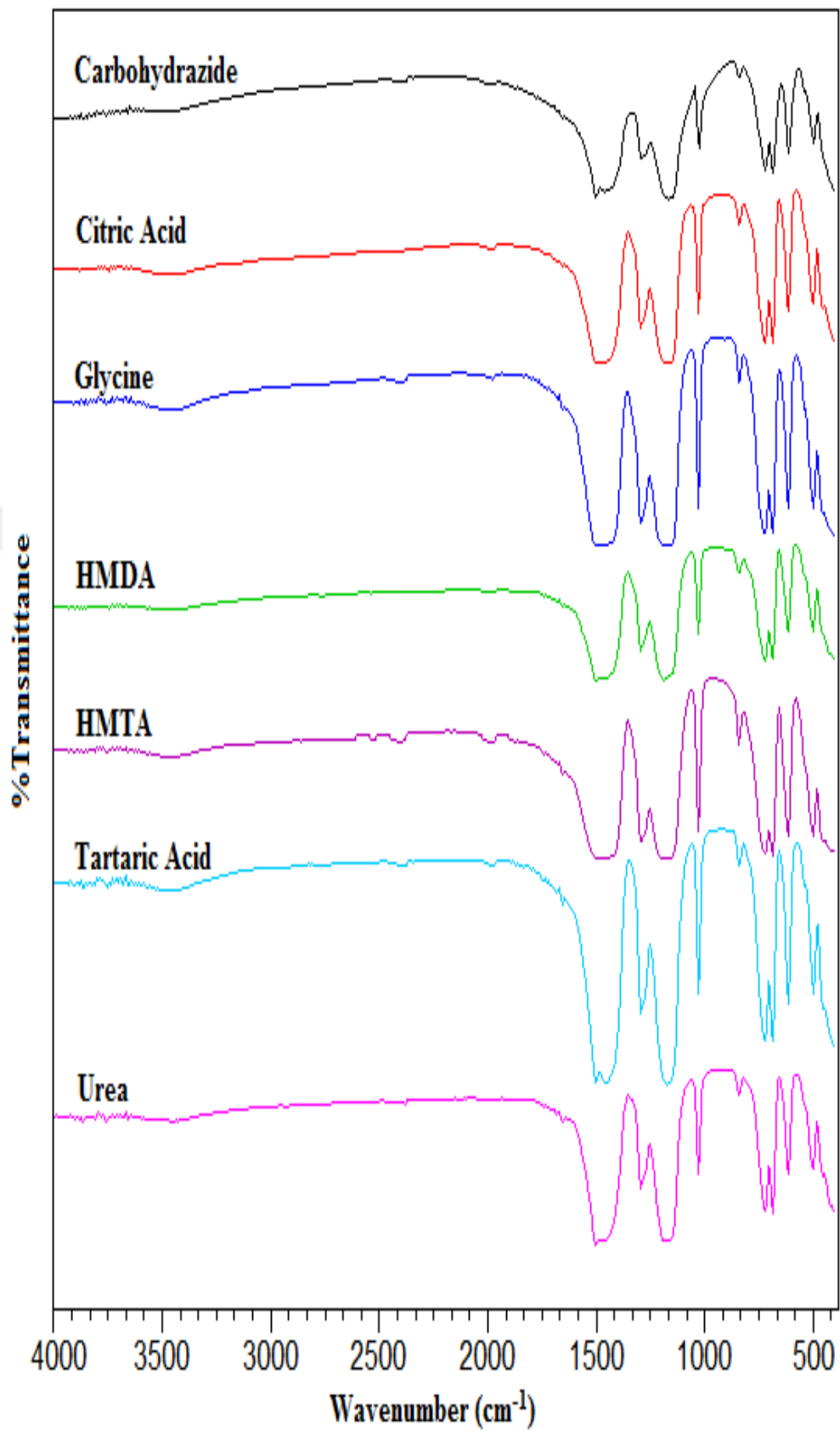


Figure 4.15. FT-IR Spectra of $Mg_2B_2O_5$ at $1000^\circ C$ Using All Fuels

4.1.1.2 Powder X-Ray Diffraction (PXRD) Studies

The assignments of the characteristic reflections of the as-prepared products were made by comparing their PXRD patterns with the International Center for Diffraction Data (ICDD) cards. It revealed that the as prepared products were suanite, $Mg_2B_2O_5$ and had a good accordance with ICDD card No 73-2232 and 86-0531 which are triclinic and monoclinic crystal structure, respectively. Moreover, it observed that different fuels formed the products at different temperature as shown in the PXRD pattern of synthesis $Mg_2B_2O_5$ (400.5minutes) (Figure 4.16). It showed only Carbohydrazide fuel and Glycine are in a good accordance with the reported data card while the rest of products with the other fuels are in amorphous phase. These presences confirmed the consistencies of the products with the FT-IR spectra as previously displayed in Figure 4.8. The two reflections at about $2\theta=35.00^\circ$ and $2\theta=35.10^\circ$ in the pattern of $Mg_2B_2O_5$ synthesized with carbohydrazide fuel corresponds to pure triclinic $Mg_2B_2O_5$ (ICDD card no: 73-2232) with high crystallinity which indicates that reaction temperature has no significant effect on the phase purity. However, the pattern of $Mg_2B_2O_5$ product with glycine fuel refers to monoclinic $Mg_2B_2O_5$ (ICDD card no: 86-0531) since no splitting observed at $2\theta \sim 35.00^\circ$.

Figure 4.17 and 4.18 showed the PXRD patterns of the products obtained at $400^\circ C$ and $500^\circ C$, respectively and only small changed on the intensity were examined. The patterns of $Mg_2B_2O_5$ synthesized with citric acid, HMDA, HMTA and urea are still in amorphous phases. The intensities of product synthesized with carbohydrazide decrease as heating temperature increases. Meanwhile, with the same condition the intensity of product obtained with glycine fuel increases.

After further heating the products at $600^\circ C$ for an hour, the patterns of $Mg_2B_2O_5$ prepared with HMTA, HMDA and urea as fuel the reflections of $Mg_2B_2O_5$ were started to form. The products obtained with these fuels have similar reflections and are in a great accordance with ICDD card No 86-0531 (Figure 4.19) which belongs to in monoclinic phase of $Mg_2B_2O_5$. Even though the peaks in the pattern have yet formed steadily, the single sharp band at around $2\theta \sim 35^\circ$ specifies the presences of monoclinic crystal structure of $Mg_2B_2O_5$.

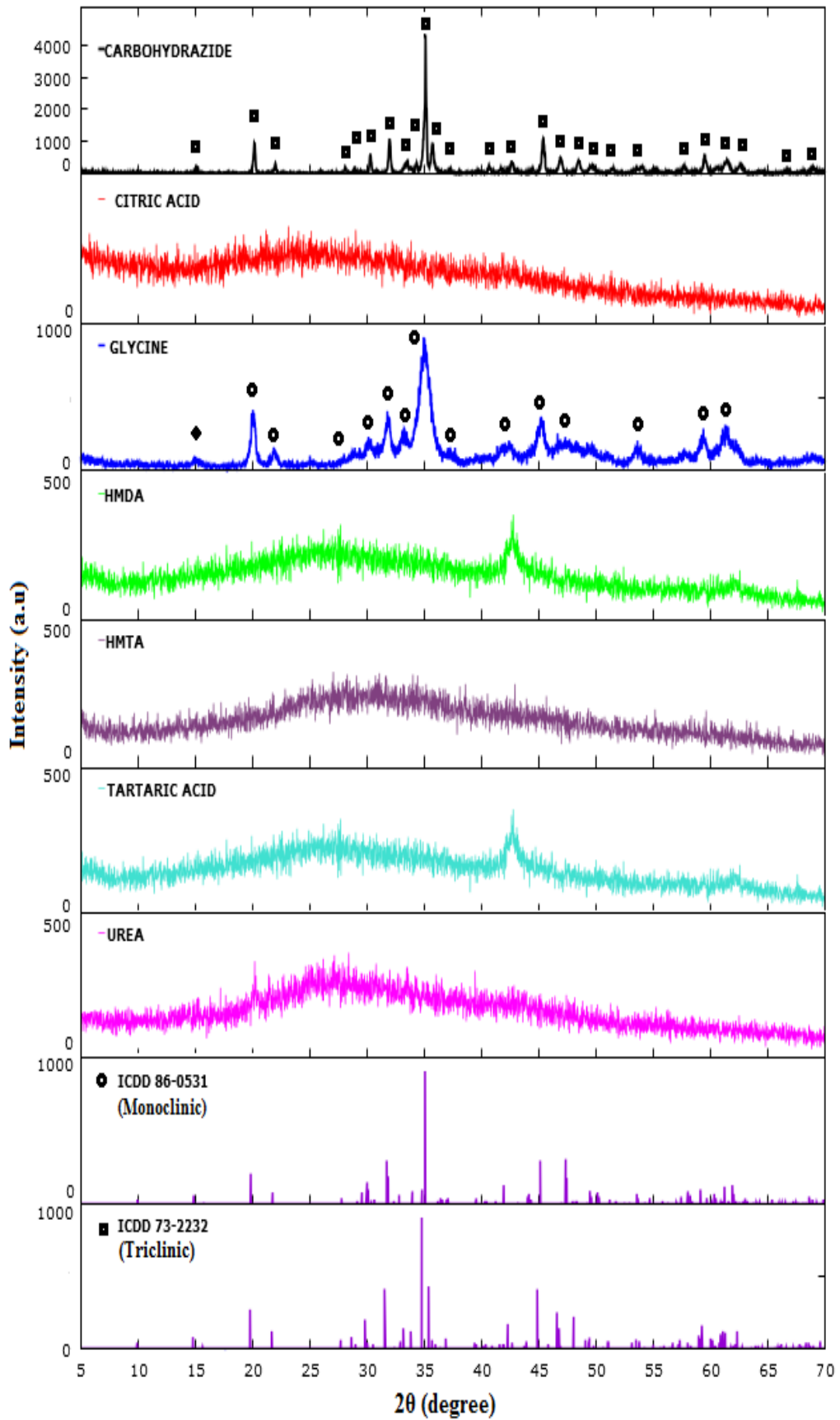


Figure 4.16. PXRD Patterns of Synthesis $Mg_2B_2O_5$ Using All Fuels

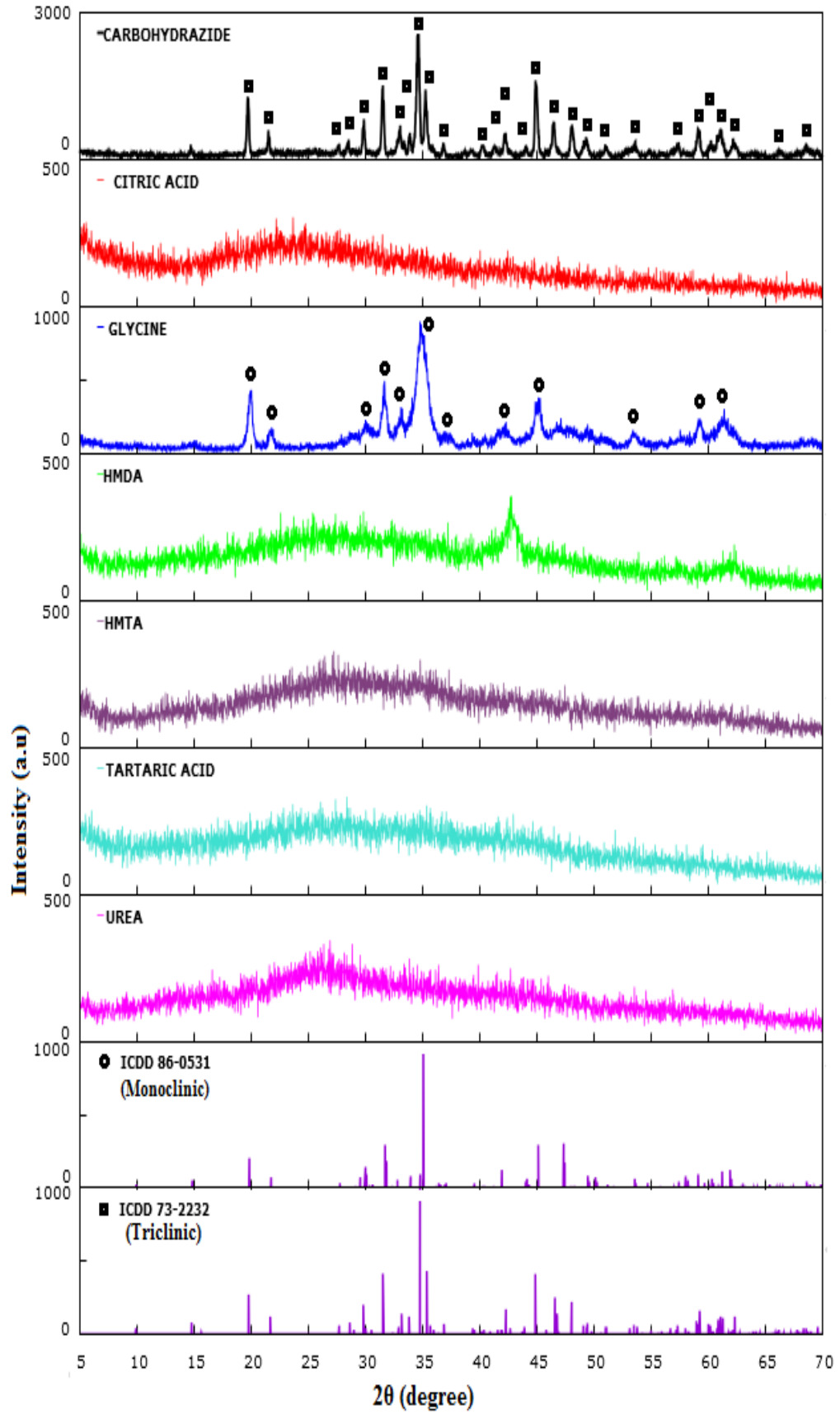


Figure 4.17. PXRD Patterns of $Mg_2B_2O_5$ Heated at $400^\circ C$ Using All Fuels

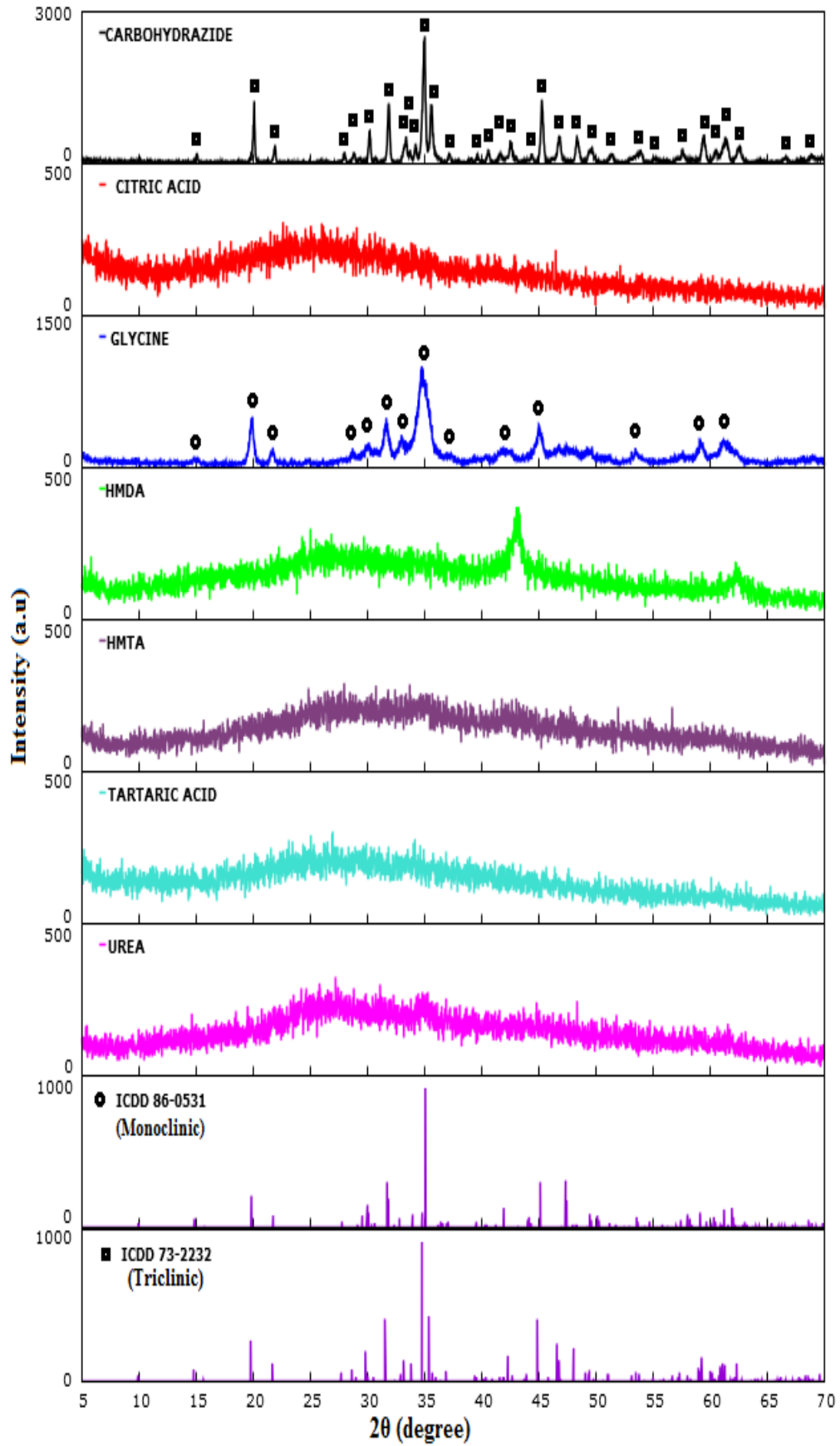


Figure 4.18. PXRD Patterns of $Mg_2B_2O_5$ Heated at $500^\circ C$ Using All Fuels

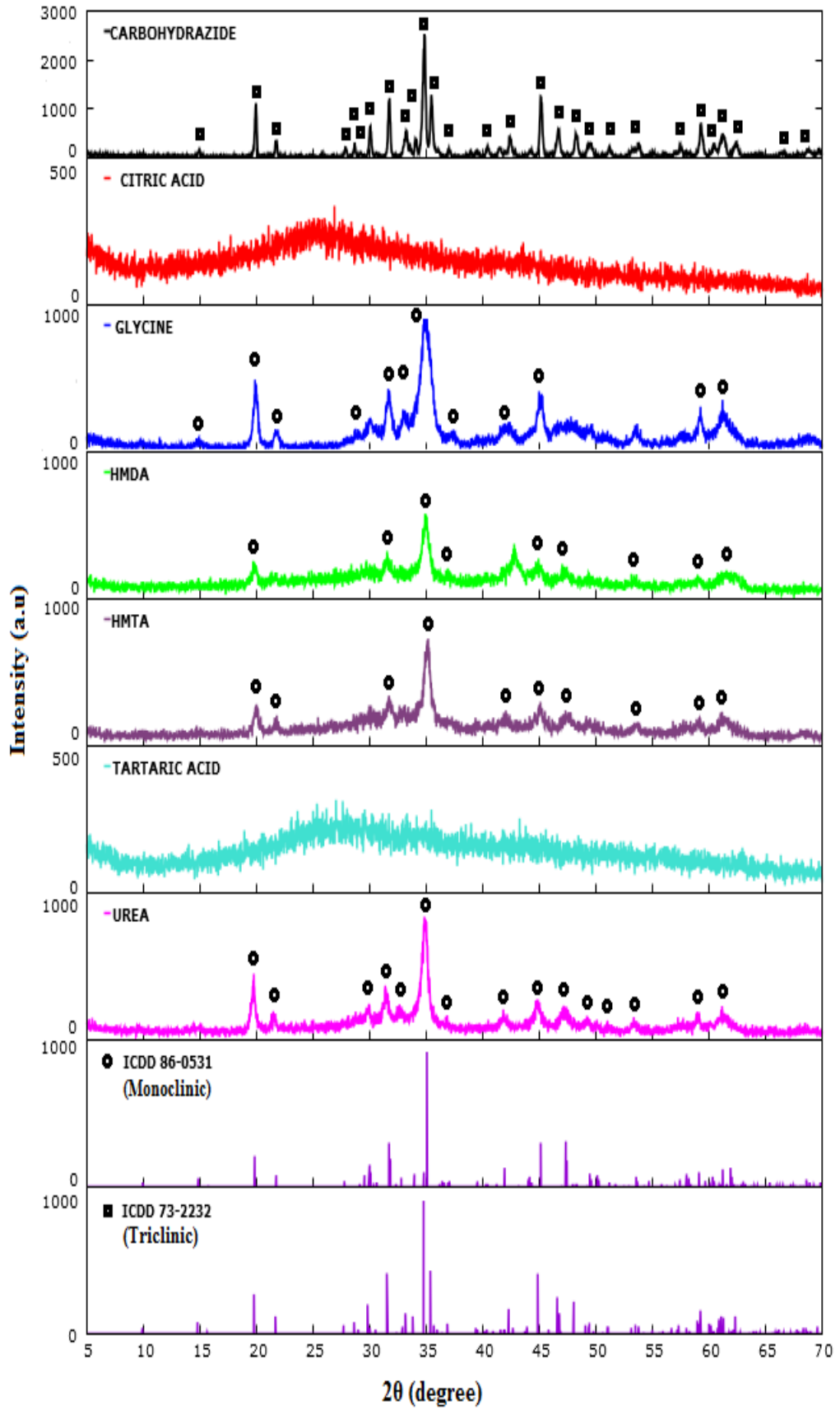


Figure 4.19. PXRD Patterns of $Mg_2B_2O_5$ Heated at $600^\circ C$ Using All Fuels

Validated the FT-IR results, the XRD patterns of the $Mg_2B_2O_5$ products were with all fuels were formed at $700^\circ C$ (Figure 4.20). These behaviors of the products proved the fuel effect and temperature effect on the formation of magnesium pyroborate since different fuel formed $Mg_2B_2O_5$ at different temperatures. It reveals that the as-prepared product of $Mg_2B_2O_5$ with citric acid fuel obtained at $700^\circ C$ assigns to monoclinic phase of $Mg_2B_2O_5$ due to the appearance of single sharp peak at about $2\theta=35.06^\circ$. In addition, the XRD pattern of product with tartaric acid fuel that obtained at $700^\circ C$ is still difficult to analyze because of its low intensity and all the peaks of $Mg_2B_2O_5$ have yet formed. Even so, the formation of $Mg_2B_2O_5$ by using tartaric acid fuel at $700^\circ C$ has confirmed by its FT-IR spectra that was shown in Figure 4.12, previously. Unlike the products with amine fuels that start forming monoclinic phases $Mg_2B_2O_5$ with higher intensity at $600^\circ C$, the transformation of monoclinic $Mg_2B_2O_5$ into triclinic $Mg_2B_2O_5$ were observed in the PXRD pattern of $Mg_2B_2O_5$ obtained with glycine and urea fuel. Although it has not clearly seen, the formation of small band beside the maximum band at around $2\theta=35.06^\circ$ verified the formation of triclinic $Mg_2B_2O_5$ and the starting temperature for the transformation between two phases of $Mg_2B_2O_5$ (Figure 4.20). Furthermore, the crystallinity of the product synthesized with carbohydrazide fuel keep decreasing as the heating temperature increases which more likely to affect its crystallite size while the products that obtained by using the others fuels has higher crystallinity as temperature increases.

Given in Figure 4.21, the PXRD patterns of products synthesized with citric acid, HMDA, HMTA, and tartaric acid have similar reflections to the monoclinic $Mg_2B_2O_5$ phase and has higher crystallinity at $800^\circ C$ than the crystallinity of the products obtained at low temperatures which indicate the temperature effect on the crystallinity of the synthesized products. It also disclosed that no transformation occurs in the products obtained with carbohydrazide fuel and the intensities of products also continue to decrease along with temperature rate. According to the PXRD pattern of the product heated at $900^\circ C$, the monoclinic phase products obtained by citric acid, HMTA, HMDA, tartaric acid fuels started to transform and have identical reflections to the triclinic $Mg_2B_2O_5$ with higher crystallinity (Figure 4.22). In the patterns of the products synthesized with citric acid, glycine and urea showed a great splitting of the single peak at $2\theta\sim 35.06^\circ$ which indicate the formation

of triclinic phases of $\text{Mg}_2\text{B}_2\text{O}_5$ and also no additional reflections were observed. Whereas, there are some reflections of monoclinic phases $\text{Mg}_2\text{B}_2\text{O}_5$ (ICDD card no : 86-0531) were composed with triclinic phase of $\text{Mg}_2\text{B}_2\text{O}_5$ in the patterns of products synthesis with HMDA and HMTA. The reflections at about $2\theta = 35.06^\circ$, $2\theta = 41.9^\circ$, and $2\theta = 47.3^\circ$ are the additional reflections that do not exist in the other patterns.

High crystallinity pure triclinic $\text{Mg}_2\text{B}_2\text{O}_5$ was obtained by further heating at 1000°C (Figure 4.23). The patterns of the products were in a great agreement with ICDD card no 73-2231 that belongs to triclinic $\text{Mg}_2\text{B}_2\text{O}_5$. However, additional reflection was observed at $2\theta = 47.3^\circ$ for the products synthesized with HMDA and HMTA fuel which belongs to monoclinic $\text{Mg}_2\text{B}_2\text{O}_5$. The existence of this reflection at 1000°C confirmed the fuel and temperature effects during this synthesis process as the monoclinic peak are slowly disappeared when temperature increases and these behaviors varies according to the type of fuels.

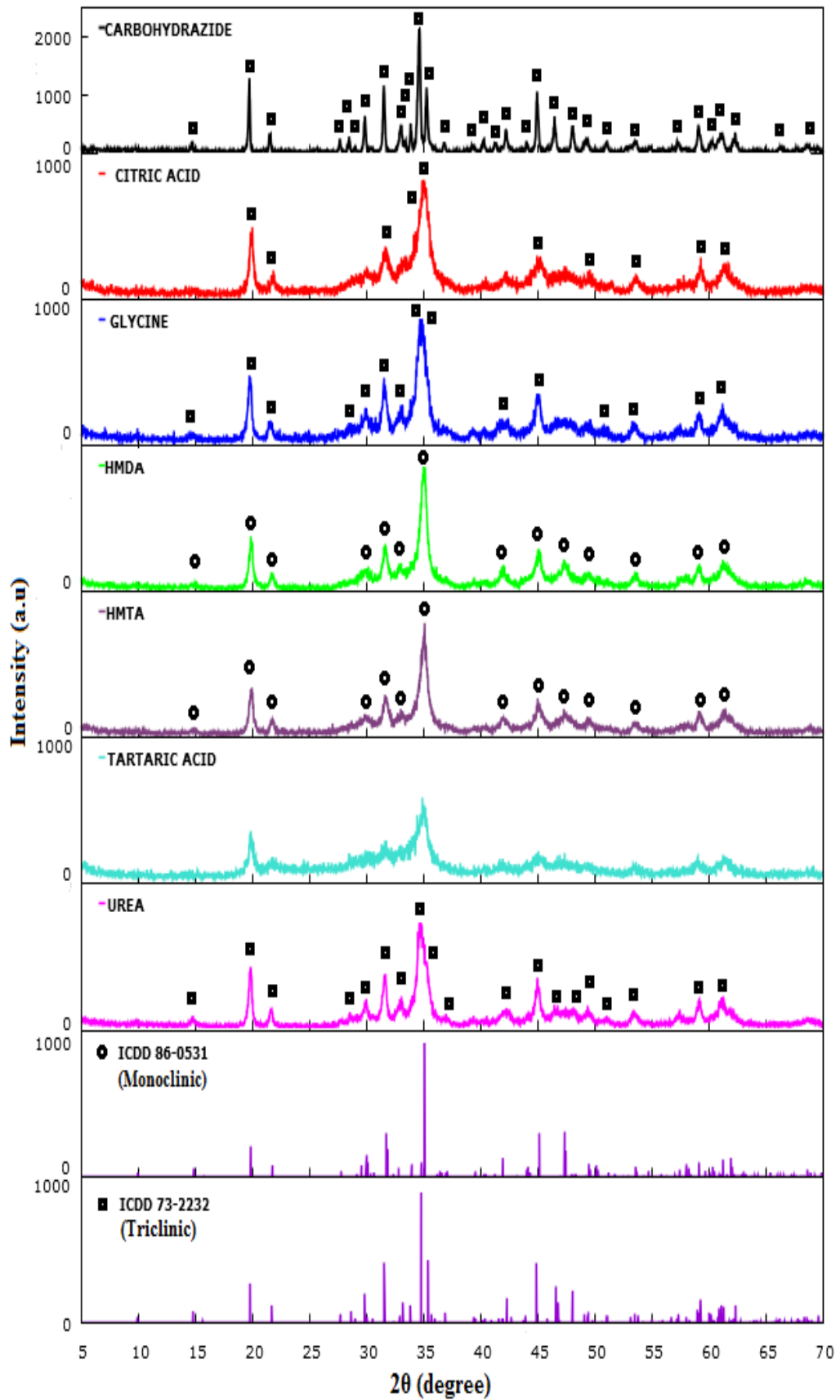


Figure 4.20. PXRD Patterns of $Mg_2B_2O_5$ Heated at $700^\circ C$ Using All Fuels

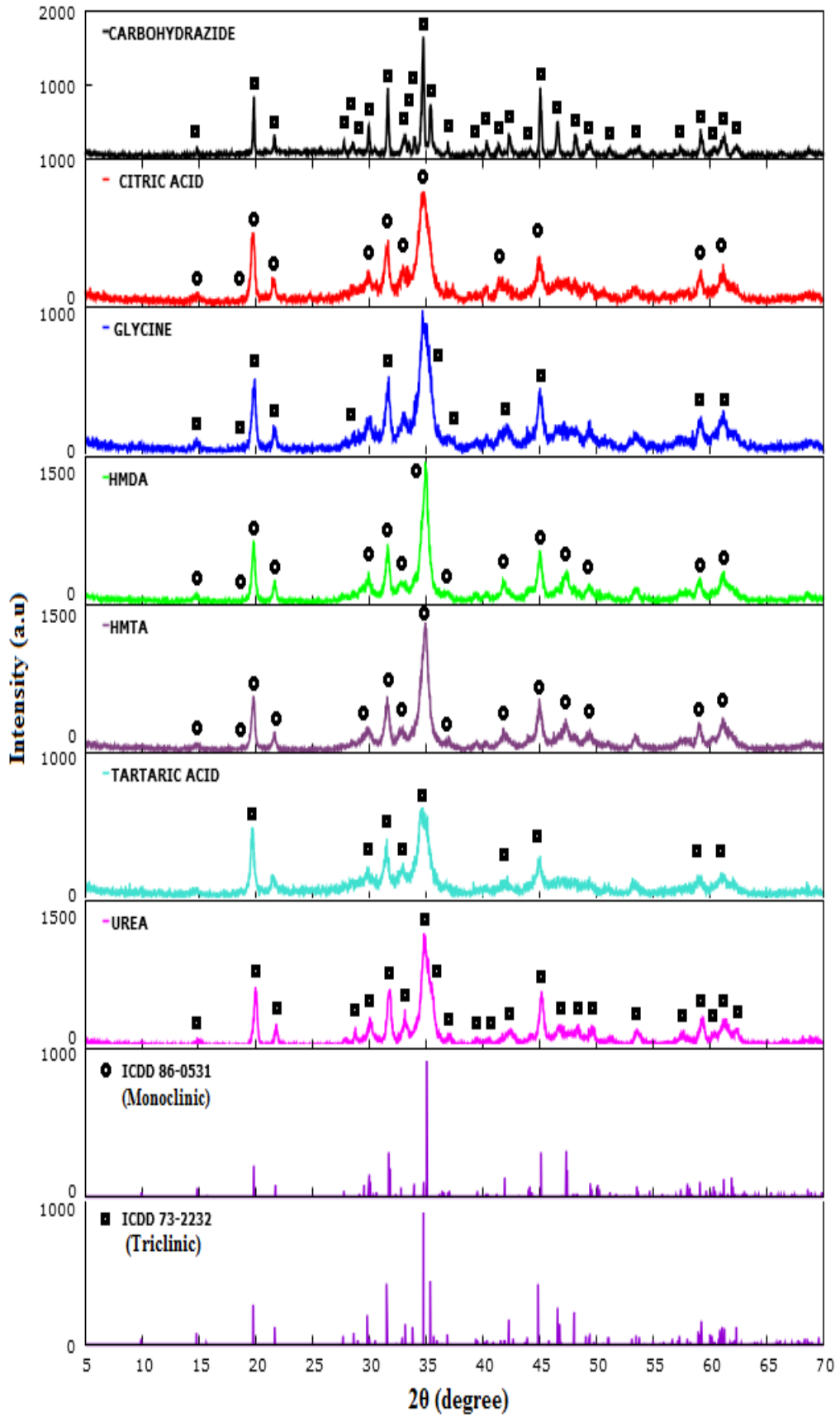


Figure 4.21. PXRD Patterns of $Mg_2B_2O_5$ Heated at $800^\circ C$ Using All Fuels

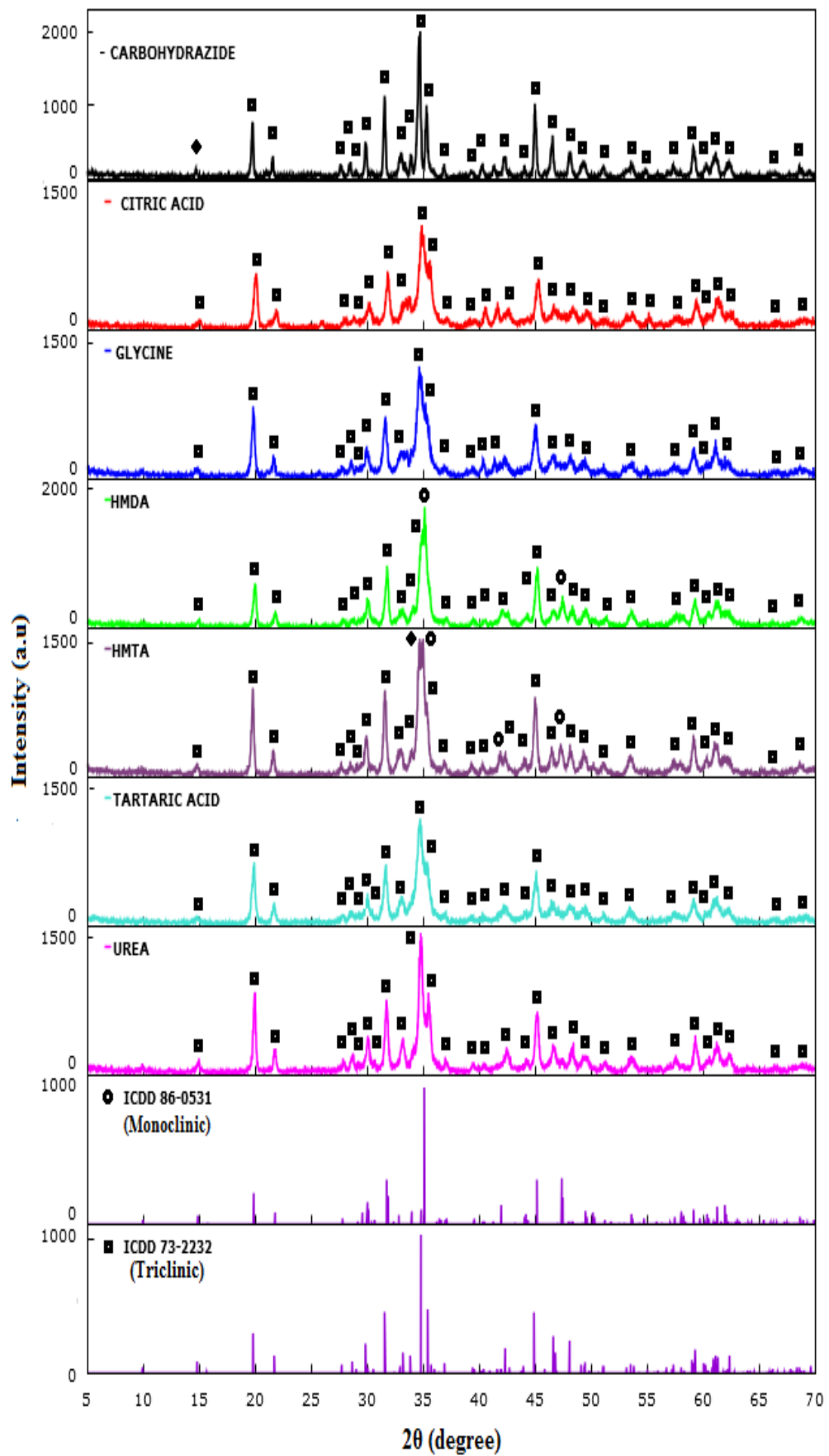


Figure 4.22. PXRD Patterns of $\text{Mg}_2\text{B}_2\text{O}_5$ Heated at 900°C Using All Fuels

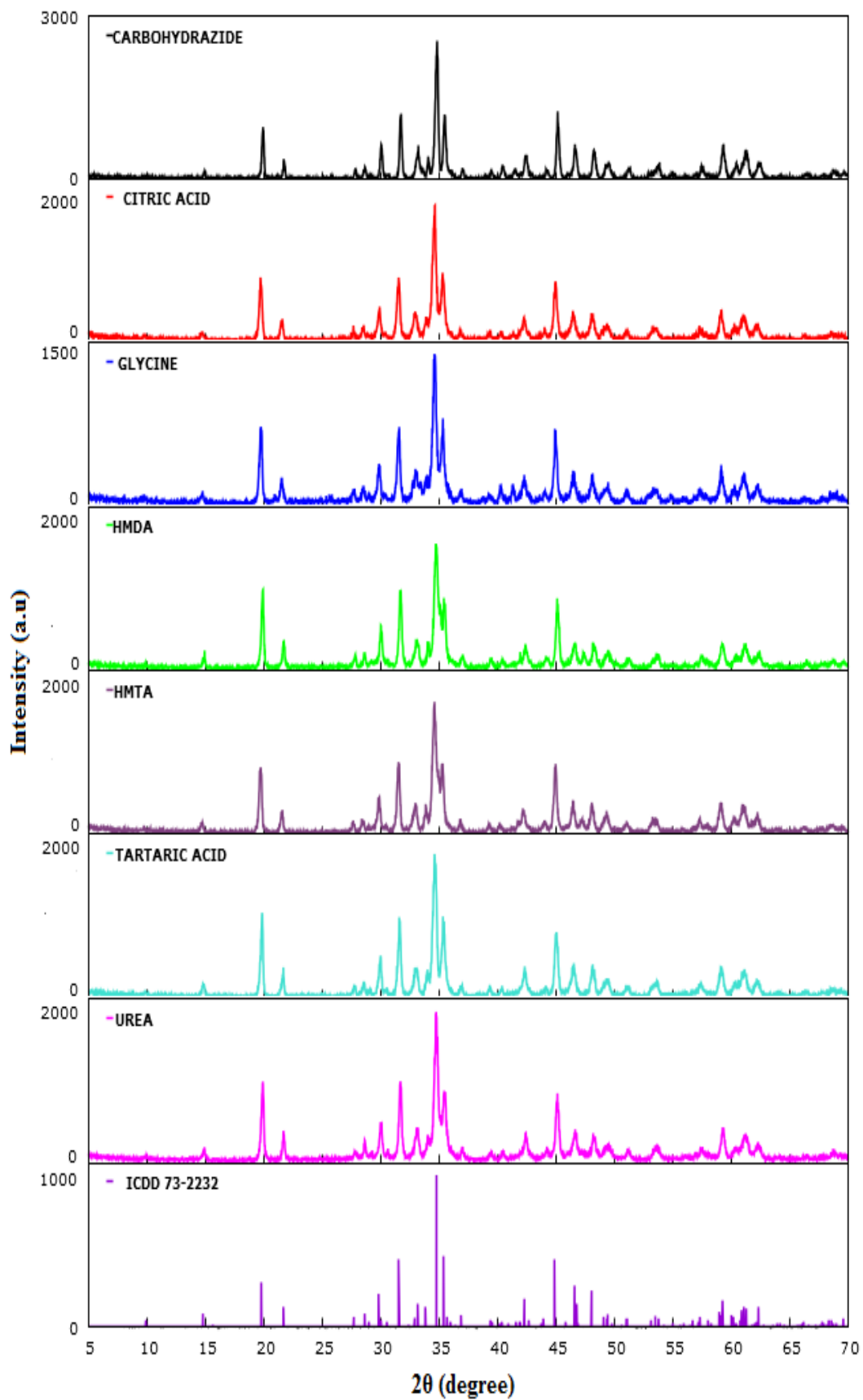


Figure 4.23. PXRD Patterns of $Mg_2B_2O_5$ Heated at $1000^\circ C$ Using All Fuels

The crystallite sizes of the pure $Mg_2B_2O_5$ were determined by using Debye-Scherrer's Equation.

$$D = \frac{K\lambda}{\beta \cos\theta}$$

Where D is the average crystallite size (nm), K is the constant shape factor that generally taken as 0.90, λ is the radiation wavelength (CuK α) which is λ equal to 1.54056 Å, β is the full width at half of the maximum (radians) and θ is the diffraction angle (Langford and Wilson, 1978; Scherrer, 1918; Uztetik Morkan and Gul, 2018).

The effect of temperature on the crystallite size of the products were shown in Table 4.3 and it observed that only the products with carbohydrazide and glycine fuel have crystallite size value at all heating temperature while the other fuels were formed in the amorphous products which lead to zero crystallite size at the temperature lower than 600°C. For these reasons, the crystallite sizes of the products with all fuels were exposed in the range of 700°C to 1000°C as shown in Figure 4.24.

Table 4.3. Crystallite Size of $Mg_2B_2O_5$

Fuel	Crystallite size (nm)							
	Syn	400°C	500°C	600°C	700°C	800°C	900°C	1000°C
CH	43.30	31.54	38.14	34.92	40.22	40.98	35.59	34.09
CA	---	---	---	---	9.96	18.39	18.30	24.92
Glycine	13.22	14.64	14.68	13.41	14.99	15.67	18.60	27.76
HMDA	---	---	---	11.35	15.94	18.74	21.47	26.23
HMTA	---	---	---	13.59	15.81	17.61	24.98	25.35
TA	---	---	---	---	15.41	17.35	18.48	28.64
Urea	---	---	---	17.36	17.48	19.63	24.50	26.31

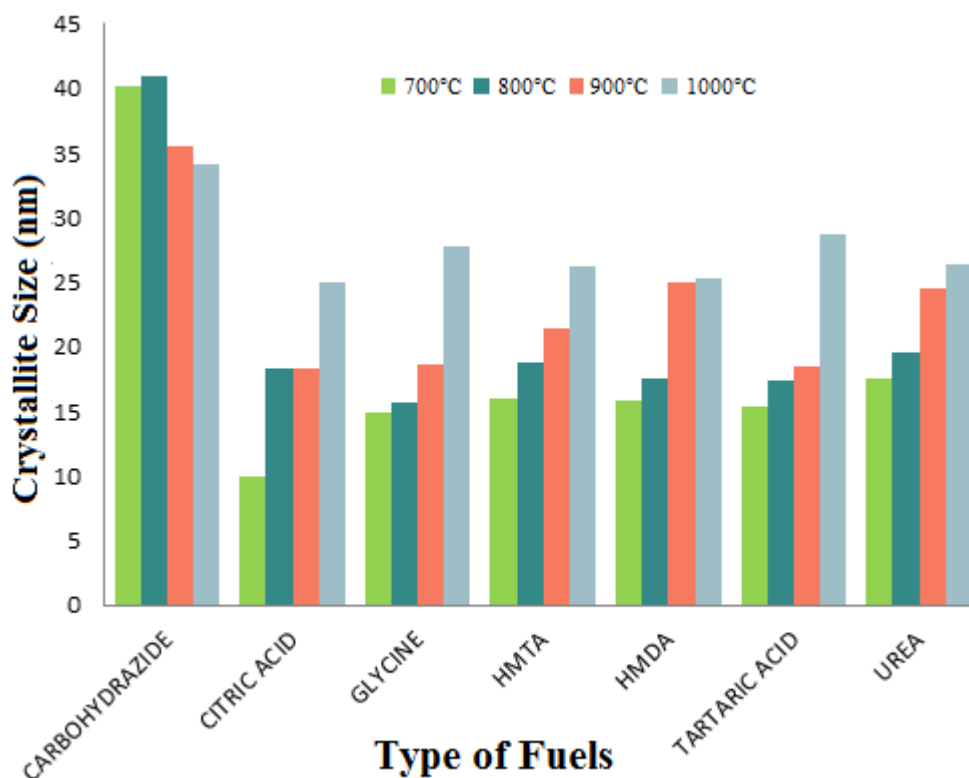


Figure 4.24. Crystallite Size of $Mg_2B_2O_5$ Obtained at 700°C-1000°C

Given in the graph above, it showed that only the products that are synthesized with carbohydrazide decreases its crystallite size as the temperature increases while the crystallite size of the products obtained by using the rest of the fuels increase by increasing the temperature. Despite of these behaviors, carbohydrazide fuel has the highest crystallite size at 1000°C with 34.09 nm and the lowest was 24.92 nm, which belongs to the products by using citric acid as fuel. Furthermore, these behaviors also confirmed the relationship of intensities of the PXRD patterns with the crystallite size values of the products since the crystallite size are increase as the intensities of the PXRD patterns increase and vice versa.

4.1.1.3 UV-VIS Spectroscopy Studies

The optical characteristics of pure $Mg_2B_2O_5$ were also determined by using UV-VIS Spectrophotometer in the range of wavelength 900-200 nm. The optical band gap energy of as-prepared products with each fuel were examine by plotting the $(\alpha h\nu)^2$ versus energy which also known as Tauc plot. Tauc plot was plotted for the products that were obtained at 800°C and 900°C, which are the transformation temperature of $Mg_2B_2O_5$ and also for single phase of triclinic $Mg_2B_2O_5$ was obtained at 1000°C. The graphs were plotted by using the UV-VIS absorbance data and the optical band gap energy was attained by taking the intercept of the curve on the energy in the x-axis (Tauc, 1968; Viezbicke, 2015).

The wavelength of products synthesized by using each fuels are listed in Table 4.4 and 4.5 for absorbance and reflectance data, respectively. From the tables, it noted that when the heating temperature increases the wavelength of both absorbance and reflectance spectra of the products decrease. These decrescence in wavelength values indicated that the products are blue shifted. It also shown that the absorbance and reflectance of the spectra are differ as different fuels applied and only products with urea fuel shows an increases in absorbance along with the increases of temperature. Meanwhile, the other fuels showed the increased in temperature in 900°C and decrease at 1000°C.

Table 4.4. UV-VIS Absorbance Spectra Wavelength of $Mg_2B_2O_5$

$Mg_2B_2O_5$	800°C		900°C		1000°C	
	A	Wavelength (nm)	A	Wavelength (nm)	A	Wavelength (nm)
CH	0.33	360.54	0.34	358.06	0.08	337.19
CA	0.05	384.53	0.10	380.53	0.01	337.66
Glycine	0.08	390.84	0.10	381.56	0.02	339.30
HMDA	0.11	388.99	0.17	374.19	0.15	334.91
HMTA	0.05	392.36	0.20	370.68	0.10	339.42
TA	0.27	390.91	0.08	385.13	0.02	341.01
Urea	0.17	387.72	0.20	370.06	0.25	331.51

Table 4.5. UV-VIS Reflectance Spectra Wavelength of Mg₂B₂O₅

Mg ₂ B ₂ O ₅	800°C		900°C		1000°C	
	%R	Wavelength (nm)	%R	Wavelength (nm)	%R	Wavelength (nm)
CH	40.62	390.92	46.78	380.57	82.81	338.41
CA	91.62	391.07	79.45	380.22	99.50	338.06
Glycine	83.43	370.20	78.27	369.5	92.76	337.25
HMDA	80.35	381.62	67.73	373.45	70.56	334.44
HMTA	88.60	391.37	62.53	369.72	89.19	338.83
TA	65.43	391.52	82.77	384.89	95.50	340.49
Urea	67.03	370.65	63.36	369.18	57.12	331.57

The UV-VIS absorbance and reflectance spectra of Mg₂B₂O₅ with seven different fuels at 800°C, 900°C and 1000°C are shown in Figure below. At the same temperature the products with various organic fuels give similar spectra of optical properties. The UV-VIS absorbance and reflectance spectra of the as-prepared products at 800°C gave the band at the ultraviolet region around 270 nm and at around 390 nm as shown in Figure 4.25 and Figure 4.26.

The products obtained at 900°C also showed the similar spectra and the two main bands at UV-region around 260 nm and 380 nm (Figure 4.27 and 4.28). Meanwhile, given in Figure 4.29 and 4.30 there were two intense peaks were observed at 250 nm and 340 nm for the products synthesized at 1000°C.

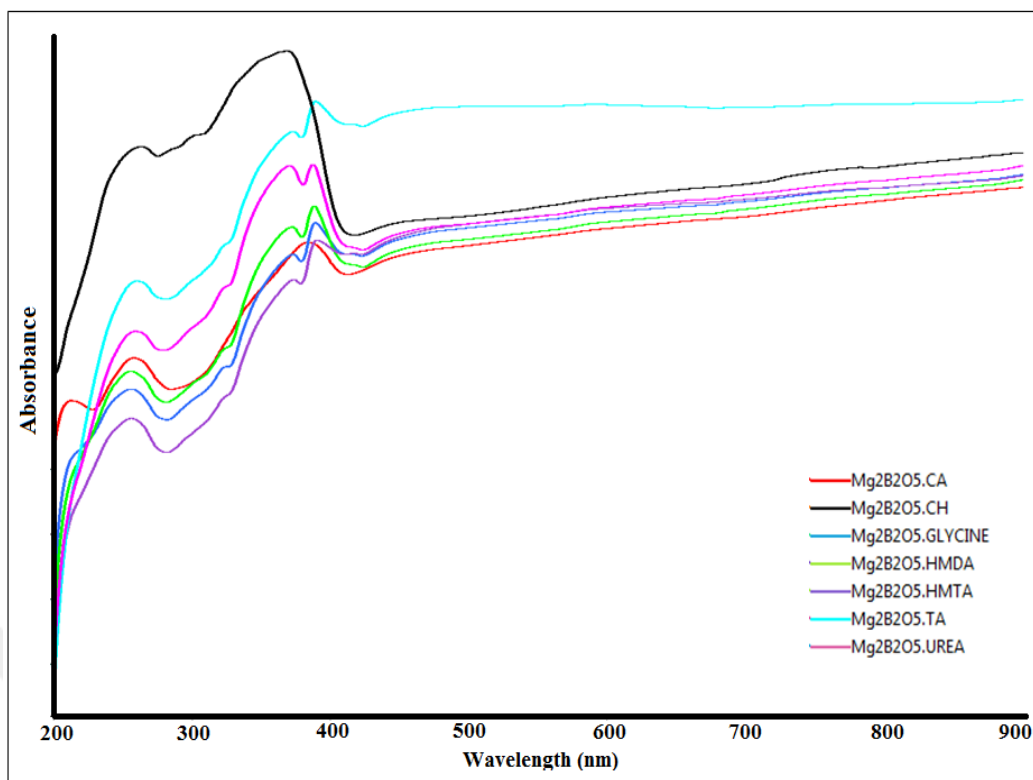


Figure 4.25. UV-VIS Absorbance Spectra of $Mg_2B_2O_5$ at $800^\circ C$

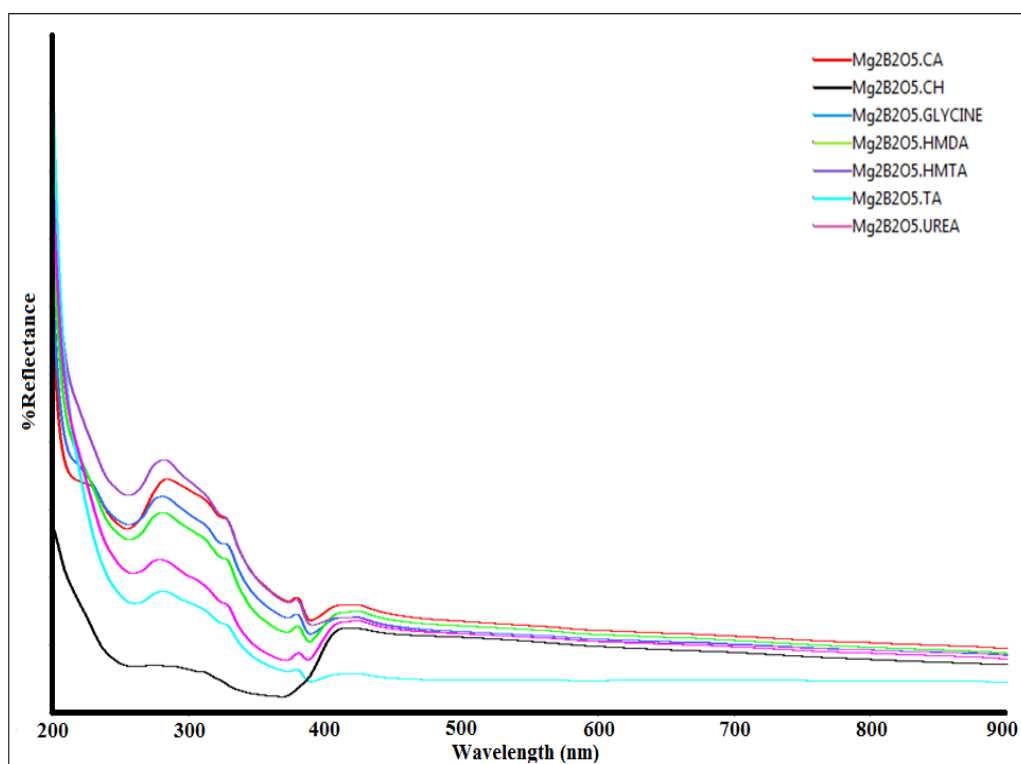


Figure 4.26. UV-VIS Reflectance Spectra of $Mg_2B_2O_5$ at $800^\circ C$

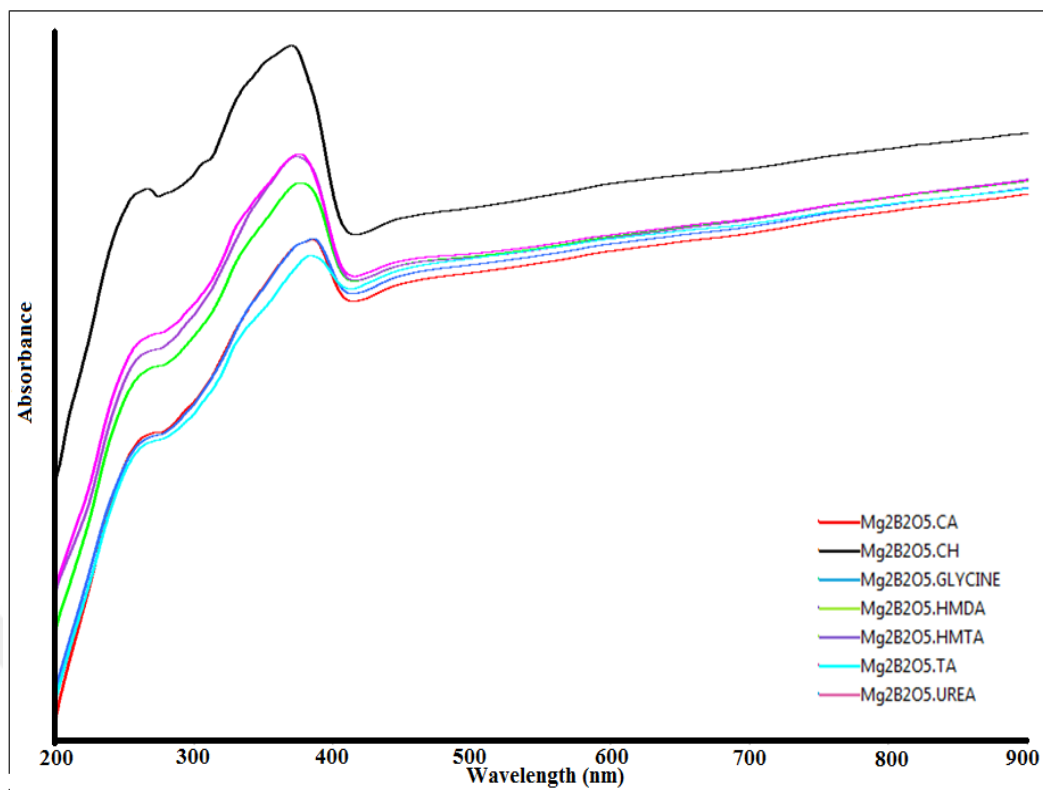


Figure 4.27. UV-VIS Absorbance Spectra of $Mg_2B_2O_5$ at $900^\circ C$

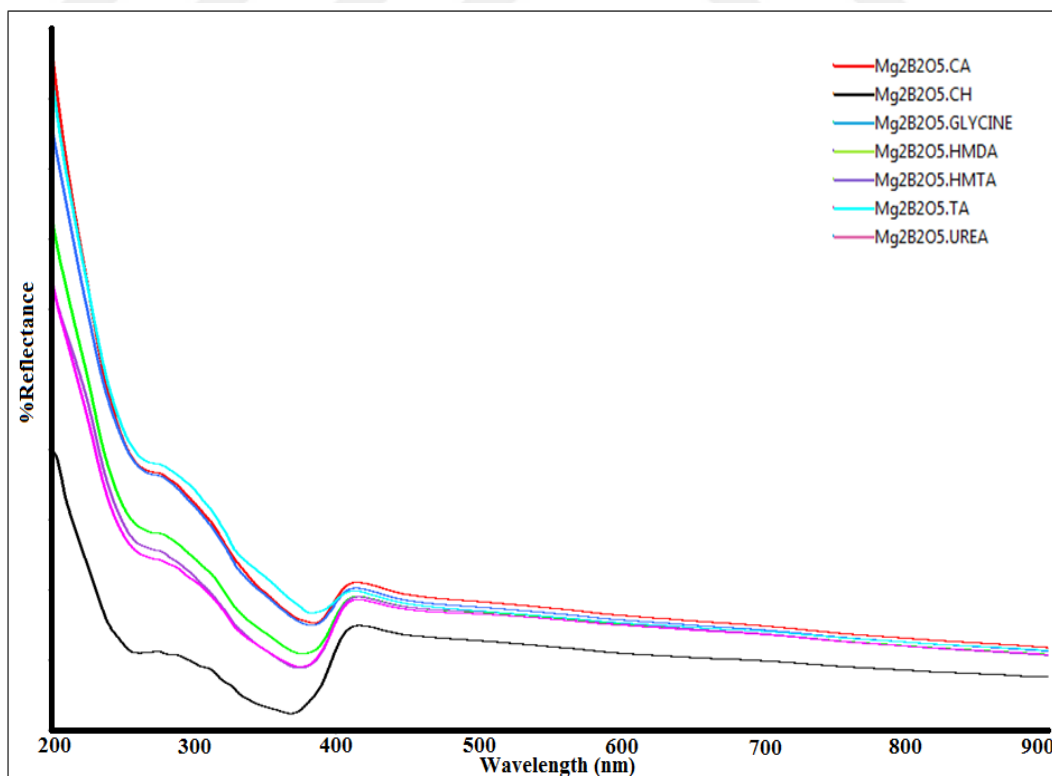


Figure 4.28. UV-VIS Reflectance Spectra of $Mg_2B_2O_5$ at $900^\circ C$

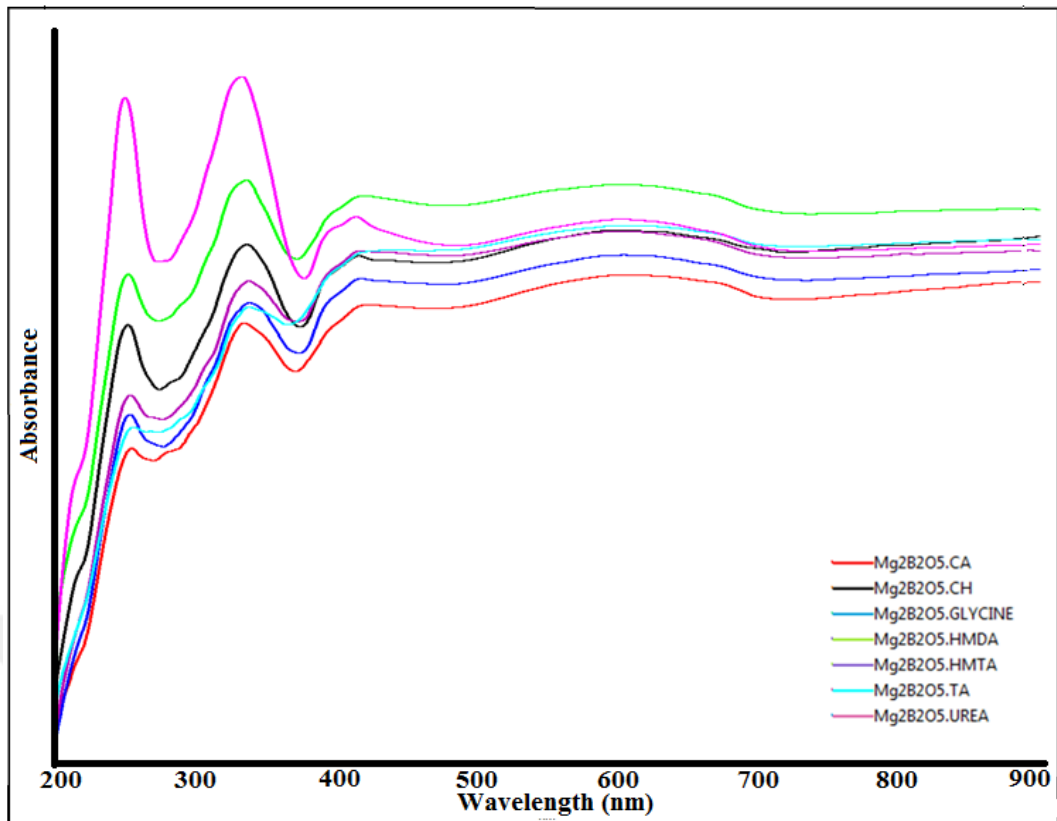


Figure 4.29. UV-VIS Absorbance Spectra of $Mg_2B_2O_5$ at $1000^\circ C$

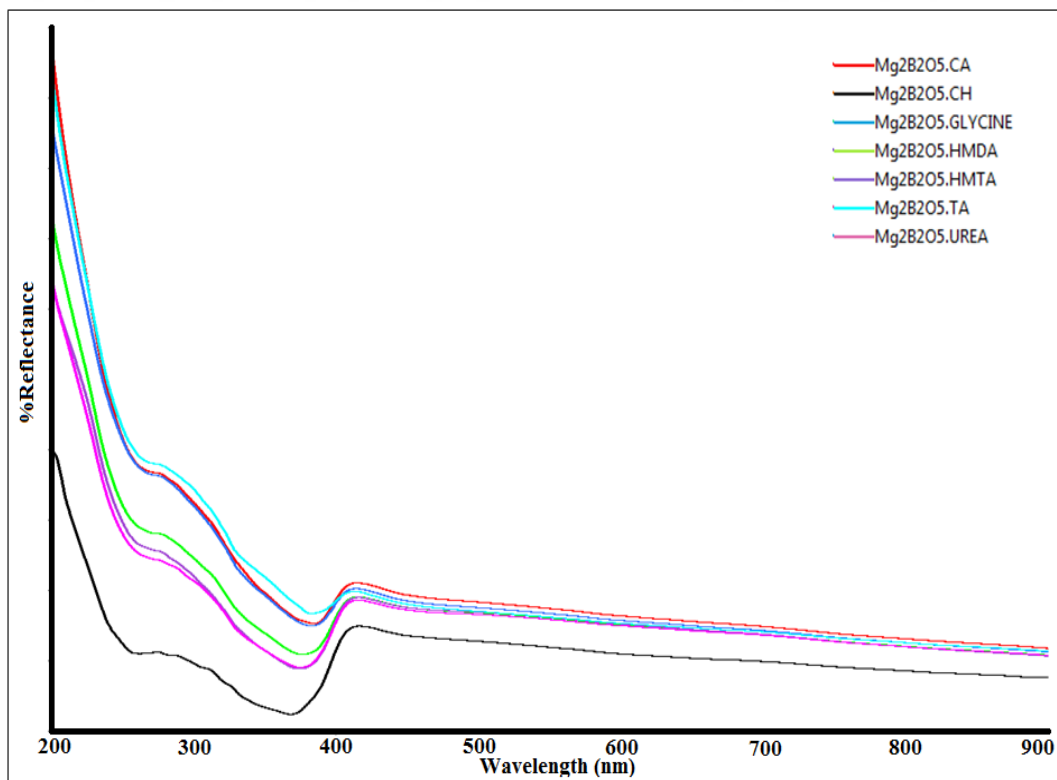


Figure 4.30. UV-VIS Reflectance Spectra of $Mg_2B_2O_5$ at $1000^\circ C$

For all these temperatures, It can be clearly seen that the absorbance bands are only observed at wavelength ranges of 250-400 nm while there is no bands were examined after 400 nm. These great transparencies of the products on the visible region due to the small size of magnesium ions that contained in the products which only have two electrons in the s-orbital of the valence shell. For this reasons, the excitation of energy needs higher energy and emits light only in the ultraviolet regions.

The optical band gap energy of as-prepared product at 800°C, 900°C and 1000°C were determined using UV-VIS absorbance data by taking the intercept of the curve on the energy in the x-axis of Tauc plot. Comparing all of these results, it is obviously showed that the optical band gap energy of the products are decrease with the increase in temperature (Figure 4.31).

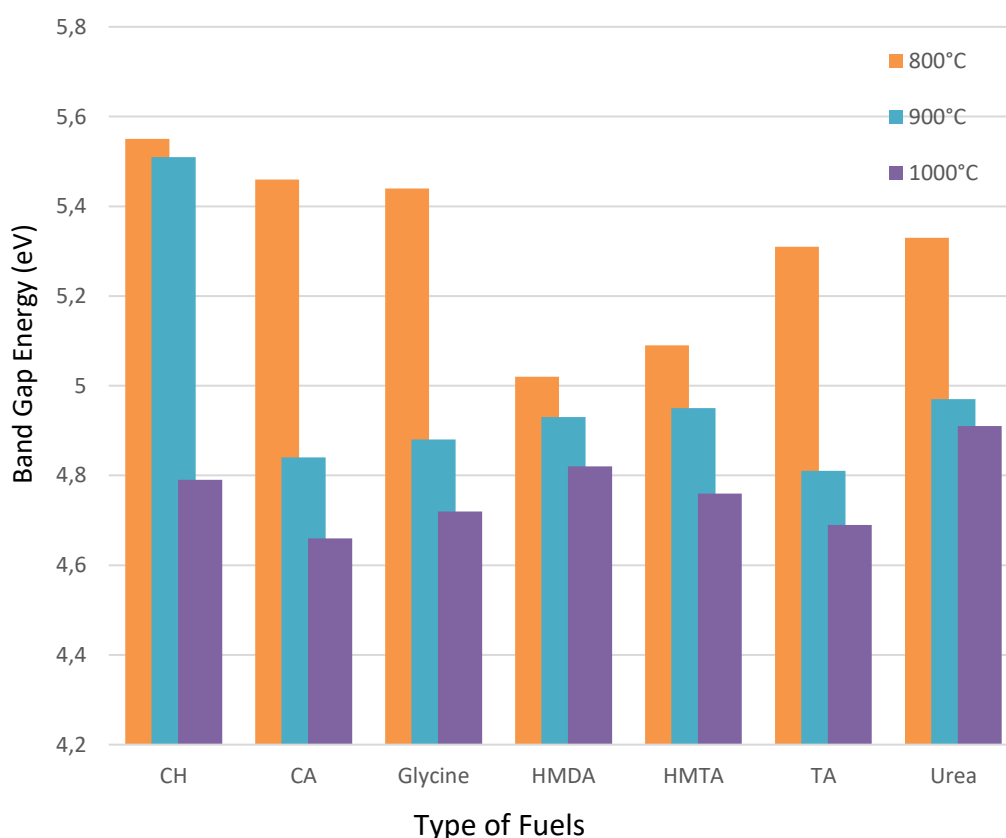


Figure 4.31. Optical Band Gap Energy of $Mg_2B_2O_5$ obtained at 800°C-1000°C

Specifically, as shown in Figure 4.32, the optical band gap are in the range 5.00-5.55 eV for the products obtained at 800°C and 4.80-5.51 eV for the products obtained at 900°C (Figure 4.33). Furthermore, the optical band gap energy of the products obtained at 1000°C was in the range 4.65 and 4.91 eV (Figure 4.34). The band gap energy that of products acquired at 1000°C have near to the results that were obtained by Doşler et al. (2010) which is 4.72 eV as given in Table 4.6.

Table 4.6. Optical Band Gap Energy of Pure Mg₂B₂O₅

Temperature	Band Gap (eV)						
	CH	CA	Glycine	HMDA	HMTA	TA	Urea
800°C	5.55	5.46	5.44	5.02	5.09	5.31	5.33
900°C	5.51	4.84	4.88	4.93	4.95	4.81	4.97
1000°C	4.79	4.66	4.72	4.82	4.76	4.69	4.91

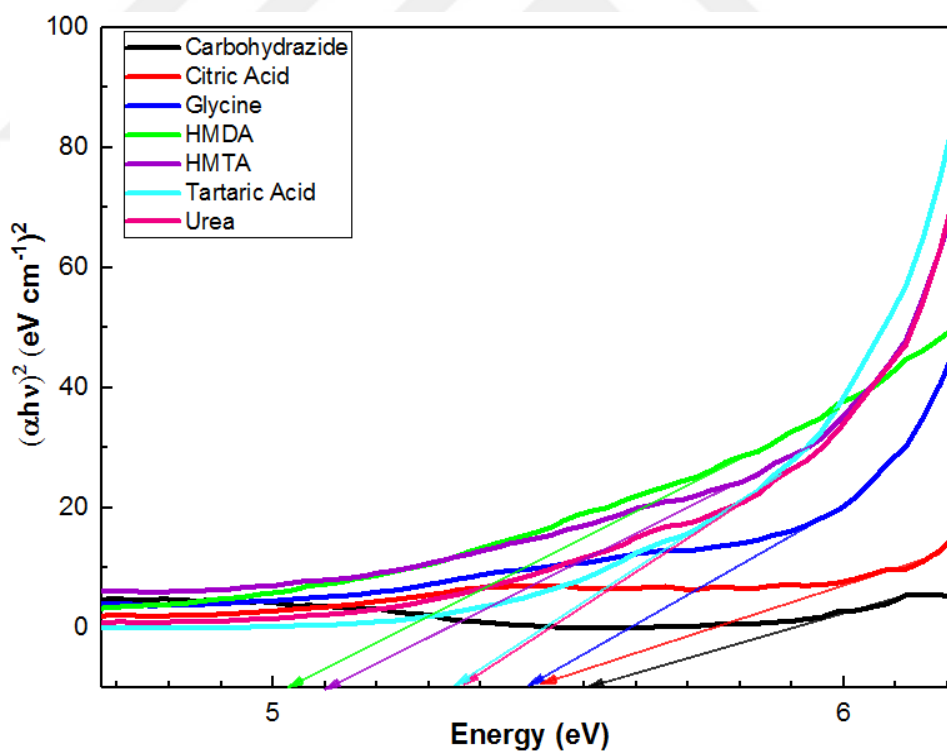


Figure 4.32. Optical Band Gap Energy of Mg₂B₂O₅ at 800°C

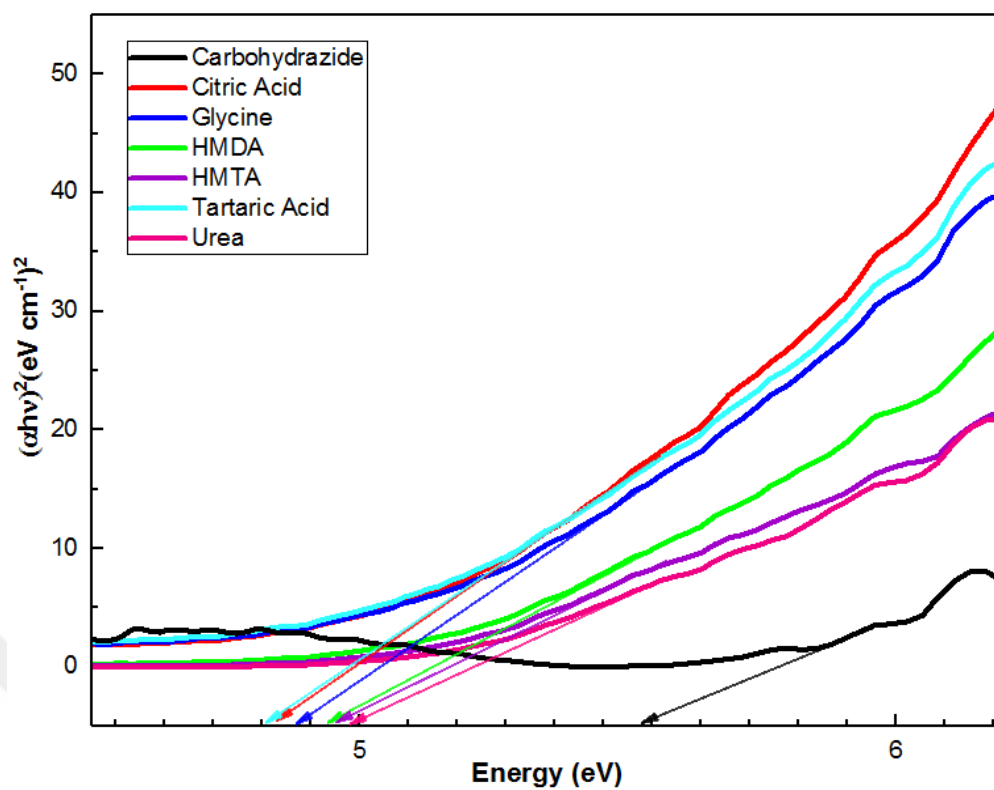


Figure 4.33. Optical Band Gap Energy of $Mg_2B_2O_5$ at $900^\circ C$

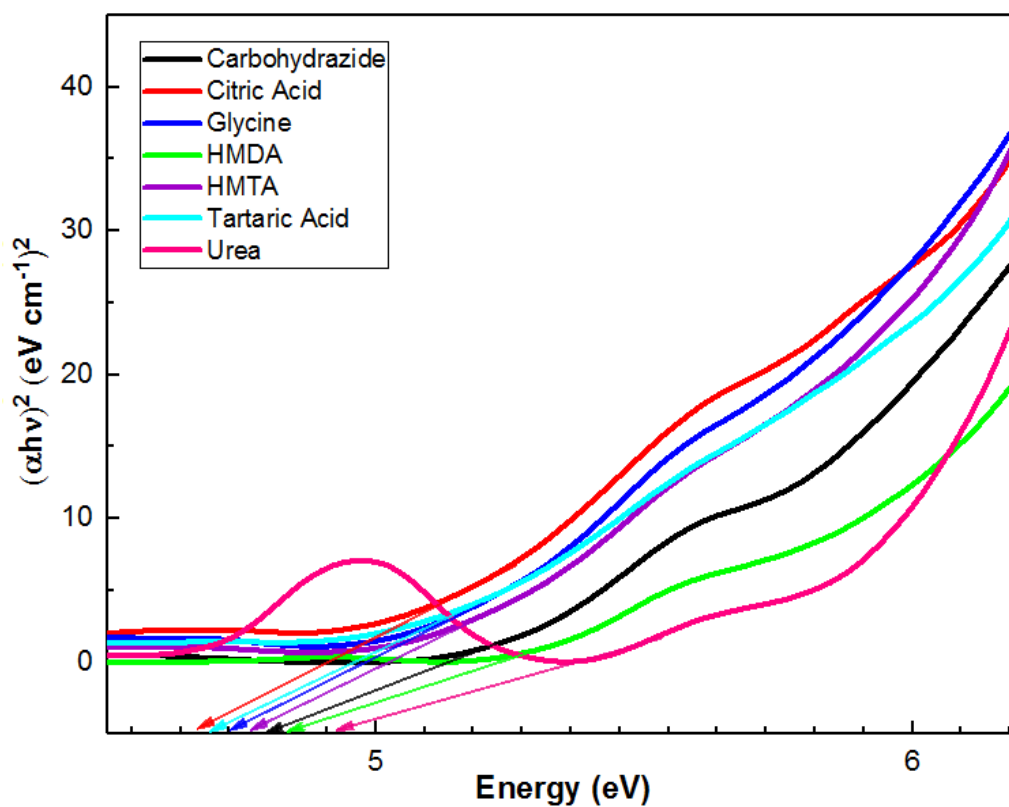


Figure 4.34. Optical Band Gap Energy of $Mg_2B_2O_5$ at $1000^\circ C$

5. CONCLUSIONS

Single phase $Mg_2B_2O_5$ were successfully synthesized via simple yet energy and time efficiency method, Solution Combustion Synthesis (SCS). The pure products were obtained in a very short time since the heating processes were only done in an hour for each temperature. In XRD studies, it was observed that the products synthesized with carbohydrazide are in triclinic phases and no monoclinic phases were observed. Moreover, the products with the other fuels formed monoclinic phase of $Mg_2B_2O_5$ at $800^\circ C$ and transformed into triclinic phase at $900^\circ C$. The results indicated that the pure triclinic $Mg_2B_2O_5$ can be acquired by heating the as-prepared products at $1000^\circ C$ although for the products with HMDA and HMTA as fuels minor reflections of monoclinic $Mg_2B_2O_5$ were detected.

The effects of fuels and temperatures on the structural properties of $Mg_2B_2O_5$ and on the crystallinities of the as-prepared products were well examined by analyzing the PXRD patterns. It was confirmed that except for the product synthesized with carbohydrazide fuel, the products obtained with Citric acid, glycine, HMDA, HMTA, tartaric acid and urea increases their crystallinity as well as the crystallite size while heating temperature increases.

In the analysis of infrared spectra, the formation of magnesium pyroborate was confirmed by observing of the bands around 680 cm^{-1} and 720 cm^{-1} represent to the B-O-B bending and the bands assigned at 1175 cm^{-1} , 1290 cm^{-1} and 1490 cm^{-1} belong to stretching vibrations of trigonal BO_3 .

Through UV-VIS analysis it was found that the optical band gap energy was decreasing as temperature increasing and the absorbance and reflectance spectra of the products only observed in the ultraviolet region and all of the products are blue shift due to the decreases in the wavelength. The calculated optical band gap energy of the products obtained at $1000^\circ C$ was attained at range of 4.66-4.91 eV for different fuels. The lowest band gap of $Mg_2B_2O_5$ was detected for citric acid fuel whereas highest value was found for urea fuel.

6. REFERENCES

- Altuntaş Öztaş N and Erdoğan H (2009) "Synthesis and Characterization of Magnesium Pyroborate by Solution Combustion and Conventional Ceramic Methods: A Comparative Study". *Z. Für Anorg. Allg. Chem.* 635:1626–1632.
- Benelmekki, M (2015) "An Introduction to Nanoparticles and Nanotechnology", *Designing Hybrid Nanoparticles* : 1-14.
- Block S, Burley G, Perloff A and Mason RD (1959) "Refinement of the crystal structure of triclinic magnesium pyroborate", *J. Res. Natl. Bur. Stand.* 62, 95.
- Bo SH, Grey CP and Khalifah PG (2015) "Defect-Tolerant Diffusion Channels for Mg²⁺ Ions in Ribbon-Type Borates: Structural Insights into Potential Battery Cathodes MgVBO₄ and Mg_xFe_{2-x}B₂O₅", *Chem. Mater.* 27: 4630–4639.
- Bokii, GB and Kravchenko VB (1967) "Crystal-chemical classification of borates", *J. Struct. Chem.* 7: 860–877.
- Buzea, C, Pacheco, II, and Robbie, K (2007) "Nanomaterials and nanoparticles: Sources and toxicity. *Biointerphases*, 2(4), MR17–MR71.
- Chen S, Zhang D and Sun G (2014) "In situ synthesis of porous ceramics with a framework structure of magnesium borate whiskers", *Mater.Lett.*121:206-208.
- Christian, P, Von der Kammer, F, Baalousha, M, and Hofmann, Th (2008) "Nanoparticles: structure, properties, preparation and behaviour in environmental media". *Ecotoxicology*, 17(5), 326–343.
- Coulson CA and Dingle TW (1968) "The B–O bond lengths in boron–oxygen compounds", *Acta Crystallogr. B* 24:153–155.
- Došler U, Kržmanc MM and Suvorov D (2010) "The synthesis and microwave dielectric properties of Mg₃B₂O₆ and Mg₂B₂O₅ ceramics", *J. Eur. Ceram. Soc.* 30, 413–418.
- Elssfah EM, Elsanousi A, Zhang J, Song HS and Tang C (2007) "Synthesis of magnesium borate nanorods", *Mater. Lett.* 61, 4358–4361.
- Emeléus HJS, AG (1982) "Advances in Inorganic Chemistry and Radiochemistry" Volume 25. Academic Press, New York, N.Y.
- Fan G, Zhou H and Chen X (2017) "Optimized sintering temperature and enhanced microwave dielectric performance of Mg₂B₂O₅ ceramic", *J. Mater. Sci. Mater. Electron.* 28, 818–822.

- Fernandes JC, Guimarães RB, Continentino MA, Rapp R, Tholence JL, Dumas J, Blancquaert Y, Yates S and Paulsen C (2004) "Low-temperature properties and ESR in the quasi-one-dimensional random compound MnMgB_2O_5 ", *Phys. Rev. B* 69, 054418.
- Glass HFJ, Liu Z, Bayley PM, Suard E, Bo SH, Khalifah PG, Grey CP and Dutton SE (2017) " $\text{Mg}_x\text{Mn}_{2-x}\text{B}_2\text{O}_5$ Pyroborates ($2/3 \leq x \leq 4/3$): High Capacity and High Rate Cathodes for Li-Ion Batteries", *Chem. Mater.* 29: 3118–3125.
- Guo GC, Cheng WD, Chen JT, Huang JS and Zhang QE (1995a) "Triclinic $\text{Mg}_2\text{B}_2\text{O}_5$ ", *Acta Crystallogr. C* 51, 351–353.
- Guo GC, Cheng WD, Chen JT, Zhuang HH, Huang JS and Zhang QE(1995b) "Monoclinic $\text{Mg}_2\text{B}_2\text{O}_5$ ", *Acta Crystallogr. C* 51: 2469–2471.
- Horikoshi, S., & Serpone, N. (2013). Introduction to Nanoparticles. In S. Horikoshi & N. Serpone (Eds.), *Microwaves in Nanoparticle Synthesis* : 1–24.
- Jeevanandam, J, Barhoum, A, Chan, YS, Dufresne, A, and Danquah, MK (2018) "Review on nanoparticles and nanostructured materials: history, sources, toxicity and regulations". *Beilstein Journal of Nanotechnology*, 9:1050–1074.
- Jia HY, Huo HQ, Yan YF, Li XF, Tian MM and Chu G (2015) "Preparation of $\text{Mg}_2\text{B}_2\text{O}_5$ submicron rods by solution combustion method". *Rengong Jingti XuebaoJournal Synth. Cryst.* 44:2321–2324.
- Jiang JW, WangL, Yang Q and Yang DR (2006) "Synthesis of magnesium borate nanorods by sol-gel process". *Wuji Cailiao XuebaoJournal Inorg. Mater.* 21: 833–837.
- Karakassides MA, Petridis D, Mousdis G, Trapalis C and Kordas G (1996) "Preparation and infrared study of magnesium borate gels with a wide composition range", *J. Non-Cryst. Solids* 202: 198–202.
- Kawano T, Suehiro T, Sato T and Yamane H (2010) "Preparation, crystal structure and photoluminescence of Mn^{2+} -doped magnesium pyroborates solid solutions, $(\text{Mg}_{1-x}\text{Mn}_x)_2\text{B}_2\text{O}_5$ ", *J. Lumin.* 130, 2161–2165.
- Khan I, Saeed K, and Khan I (2017) "Nanoparticles: Properties, applications and toxicities". *Arabian Journal of Chemistry*.
- Kipcak AS, Moroydor DE and Piskin S (2013a) "Magnesium Borate Synthesis by Microwave Energy: A New Method", *J. Chem.* 2013, 1–6.
- Kipcak AS, Yilmaz BD, Moroydor DE and Piskin S (2013b) "Characterization and Neutron Shielding Behavior of Dehydrated Magnesium Borate Minerals Synthesized via Solid-State Method", *Adv. Mater. Sci. Eng.* 2013, 1–9.
- Kitamura T, Sakane K, Wada H (1988) "Formation of needle crystals of magnesium pyroborate". *J. Mater. Sci. Lett.* 7, 467–469.

- Kopp Alves A, Bergmann CP and Berutti FA (2013) "Introduction, in: Novel Synthesis and Characterization of Nanostructured Materials". Springer Berlin Heidelberg, Berlin, Heidelberg, pp. 1–9.
- Langford JJ and Wilson AJC (1978) "Scherrer after sixty years: A survey and some new results in the determination of crystallite size". *J. Appl. Crystallogr.* 11, 102–113.
- Li F, Ran J, Jaroniec M and Qiao SZ (2015) "Solution combustion synthesis of metal oxide nanomaterials for energy storage and conversion" 19.
- Li S, Fang X, Leng J, Shen H, Fan Y and Xu D (2010) "A new route for the synthesis of $Mg_2B_2O_5$ nanorods by mechano-chemical and sintering process". *Mater. Lett.* 64: 151–153.
- Li S, Xu D, Shen H, Zhou J and Fan Y (2012) "Synthesis and Raman properties of magnesium borate micro/nanorods". *Mater. Res. Bull.* 47:3650–3653.
- Li Y, Fan Z, Lu JG and Chang RPH (2004) "Synthesis of Magnesium Borate ($Mg_2B_2O_5$) Nanowires by Chemical Vapor Deposition Method". *Chem. Mater.* 16: 2512–2514.
- Liang Y, Deng A, Wang J, Shi H, Wang W and Wang L (2015) "Synthesis and growth mechanism of whisker-like $Mg_2B_2O_5$ crystals by an easy and environmentally hospitable non-aqueous ionic liquid method". *Micro Amp Nano Lett.* 10: 130–134.
- Mo ZJ, Chen, JP, Lin, J, Fan Y, Liang CY, Wang HS, Xu X.W, Hu L and Tang CC (2014) "Controllable synthesis of high aspect ratio $Mg_2B_2O_5$ nanowires and their applications in reinforced polyhydroxyalkanoate composites" *Chin. Phys. B* 23, 056201.
- Qasrawi AF, Kayed TS, Mergen A, and Gürü (2005) "Synthesis and characterization of $Mg_2B_2O_5$ ". *Mater. Res. Bull.* 40, 583–589.
- Rao CNR, Biswas K (2015) "Essentials of inorganic materials synthesis".
- Sambandan E (2008) "Inorganic Materials Chemistry: General Concept and Research Topics". iUniverse.
- Scherrer P (1918) "Nachrichten von der Gesellschaft der Wissenschaften zu Göttingen, Mathematisch-Physikalische Klasse".
- Storti E, Roso M, Modesti M, Aneziris CG, Colombo P (2016) "Preparation and morphology of magnesium borate fibers via electrospinning", *J. Eur. Ceram. Soc.* 36: 2593–2599.
- Takéuchi Y (1952) "The crystal structure of magnesium pyroborate", *Acta Crystallogr.* 5:574–581.
- Tao X and Li X (2008) "Catalyst-Free Synthesis, Structural, and Mechanical Characterization of Twinned $Mg_2B_2O_5$ Nanowires", *Nano Lett.* 8: 505–510.

- Tauc J (1968) "Optical properties and electronic structure of amorphous Ge and Si". *Materials Research Bulletin*, 3(1), 37–46.
- Uztetik Morkan A, and Gul E (2018) "Synthesis, structural characterization, and photoluminescence properties of Eu^{3+} -doped $\text{Mg}_{3-x}\text{Eu}_x(\text{BO}_3)_2$ phosphor", *International Journal of Applied Ceramic Technology*, 15(5) : 1277–1286.
- Üçyıldız A and Girgin İ (2010) "Controlled synthesis, characterization and thermal properties of $\text{Mg}_2\text{B}_2\text{O}_5$ ", *Open Chem.* 8.
- Varma A, Mukasyan AS, Rogachev AS and Manukyan KV, (2016) "Solution Combustion Synthesis of Nanoscale Materials". *Chem. Rev.* 116:14493–14586.
- Viezbicke BD, Patel S, Davis BE, and Birnie DP (2015) "Evaluation of the Tauc Method for Optical Absorption Edge Determination: ZnO Thin Films as a Model System".
- Watanabe T (1953) "Suanite, a New Magnesium Borate Mineral from Hol Kol", Suan, North Korea. *Mineral. J.* 1, 54–62.
- Weir CE and Schroeder RA (1964) "Infrared spectra of the crystalline inorganic borates". *J. Res. Natl. Bur. Stand. Sect. Phys. Chem.* 68A, 465.
- Woods WG, (1994) "An Introduction to Boron: History, Sources, Uses, and Chemistry". *Environ. Health Perspect.* 102, 7.
- Xu B, Li T, Zhang Y, Zhang Z, Liu X and Zhao J (2008) "New Synthetic Route and Characterization of Magnesium Borate Nanorods", *Cryst. Growth Des.* 8, 1218–1222.
- Xu R, Pang W and Huo Q (2011) "Modern inorganic synthetic chemistry".
- Yongdong X and Yan XT (2010) "Chemical vapour deposition: an integrated engineering design for advanced materials, Engineering materials and processes". Springer, London., New York.
- Yuan G and Xue D (2007) "Crystal chemistry of borates: the classification and algebraic description by topological type of fundamental building blocks". *Acta Crystallogr. B* 63, 353–362.
- Zampiva RYS, Venturini J, Acauan LH, Kaufmann CG, dos Santos LM, Alves AK, Bergmann CP, and CatenCS (2019) "The impact of the reaction atmosphere on the additive-free growth of $\text{Mg}_2\text{B}_2\text{O}_5$ nanorods". *Ceramic.Int.* 45:6228–6235.
- Zeng Y, Yang H, Fu W, Qiao L, Chang L, Chen J, Zhu H, Li M and Zou G (2008) "Synthesis of magnesium borate ($\text{Mg}_2\text{B}_2\text{O}_5$) nanowires, growth mechanism and their lubricating properties". *Mater. Res. Bull.* 43: 2239–2247.

- Zhu D, Nai X, Zhu C, Guo F, Bian S and Li W (2012) "Synthesis of $Mg_2B_2O_5$ whiskers via coprecipitation and sintering process". *Int. J. Miner. Metall. Mater.* 19: 969–972.
- Zhu W, Wang R, Zhu S, Zhang L, Cui X, Zhang H, Piao X and Zhang Q (2014). "Green, Noncorrosive, Easy Scale-Up Hydrothermal–Thermal Conversion: A Feasible Solution to Mass Production of Magnesium Borate Nanowhiskers". *ACS Sustain. Chem. Eng.* 2: 836–845.
- Zhu W, Xiang L, Zhang Q, Zhang X, Hu L and Zhu S(2008)"Morphology preservation and crystallinity improvement in the thermal conversion of the hydrothermal synthesized $MgBO_2(OH)$ nanowhiskers to $Mg_2B_2O_5$ nanowhiskers", *J. Cryst. Growth* 310: 4262–4267.



7. CURRICULUM VITAE

Name SURNAME :Liska Fadliyani

Place and Date of Birth : Dayah Teungoh, IDN, 25.09.1995

Universities

Bachelor's Degree : Abant İzzet Baysal University

E-mail :liskafadliyanii@gmail.com

Address :Tabaklar Mah. Hattat Emin Barın Cad. Atlas 2,
Apt No. 9 D.10, Bolu

Awards : The First of Chemistry Department,
Academic Year 2016-2017